이학박사 학위논문

애기장대 *DEMETER* 유전자의 전사 조절과 DNA demethylase 상동유전자군의 상호 작용에 대한 연구

Control of *DEMETER* Transcription and Genetic Interactions among DNA Demethylase Family Members in *Arabidopsis thaliana*

2020년 2월

서울대학교 대학원

생명과학부

박 진 섭

General Abstract

Control of *DEMETER* Transcription and Genetic Interactions among DNA Demethylase Family Members in *Arabidopsis thaliana*

Jinsup Park

School of Biological Sciences

The Graduate School

Seoul National University

The DEMETER (DME) DNA glycosylase initiates active DNA demethylation via the base-excision repair pathway and is vital for reproduction in *Arabidopsis thaliana*. DME-mediated DNA demethylation is preferentially targeted to small, AT-rich, and nucleosome-depleted euchromatic transposable elements, influencing expression of adjacent

genes and leading to imprinting in the endosperm. In the female gametophyte, *DME* expression and subsequent genome-wide DNA demethylation is confined to the companion cell of the egg, the central cell. Here, I show that in the male gametophyte, *DME* expression is limited to the companion cell of sperm, the vegetative cell, and to a narrow window of time; immediately following separation of the companion cell lineage from the germline. I define transcriptional regulatory elements of *DME* using reporter genes, showing that a small region within the *DME* gene controls its expression in male and female companion cells. *DME* expression from this minimal promoter is sufficient to rescue seed abortion and the aberrant DNA methylome associated with the null *dme-2* mutation. Within this minimal promoter, I found short, conserved enhancer sequences necessary for the transcriptional activities of *DME* and combine predicted binding motifs with published transcription factor binding coordinates to produce a list of candidate upstream pathway members in the genetic circuitry controlling DNA demethylation in

gamete companion cells. Besides I provide evidence of the minimal promoter's specific binding in yeast by a *BPC* and an HD-ZIP transcription factor. These data show how DNA demethylation is regulated to facilitate endosperm gene imprinting and potential transgenerational epigenetic regulation, without subjecting the germline to potentially deleterious transposable element demethylation.

There are several differences in *dme* mutant depending on mutation site and their ecotype. To identify what make the differences, I crossed mutants having different allele or ecotype. As a result of the crosses, I found a genomic region that seemed to be beneficial in overcoming seed abortion. In Arabidopsis there are three homologous genes of *DME*; *REPRESSOR OF SILENCING1* (*ROS1*), *DEMETER-LIKE* (*DML*) 2 and 3. These family genes are expressed in all sporophytic tissues. To address the contribution of DNA demethylation to plant life cycle and interaction between demethylases, using crosses of mutants of DNA demethylase family, I found evidence of interaction of DNA demethylase family.

Keywords: DNA demethylase, gamete companion cells, single cell-specific gene transcription, epigenetics, enhancer elements, transcription factors,

Student Number: 2008-20356

Table of Contents

List of Figures

List of Tables

Abbreviations

5' RACE	5' rapid amplification of Cdna ends
ABRC	Arabidopsis biological resource center
BPC	basic pentacysteine
CaMV	Cauliflower mosaic virus
CC	central cell
CCE	central cell element
cDNA	complementary DNA
DAG	Days after germination
DAPI	4',6-diamidino-2-phenylindole
DAP-seq	DNA affinity purification sequencing
DME	DEMETER
DML	DEMETER-LIKE
DNA	deoxyribonucleic acid
GFP	green fluorescent protein
GUS	*β-glucuronidase*

HD-ZIP	homeodomain leucine zipper
PRC2	Polycomb repressive complex 2
QE	quantitative element
qRT-PCR	Quantitative real-time polymerase chain reaction
ROS1	REPRESSOR OF SILENCING1
RT-PCR	Reverse transcription-polymerase chain reaction
SAM	Shoot apical metistem
SD	Standard deviation
SPE	sporophytic element
TE	transposable element
TU	truncated 5'UTR
UTR	untranslated region
VC	vegetative cell
VCE	vegetative cell element
WT	Wild-type

I. Chapter I.

Control of DEMETER DNA demethylase gene transcription in male and female gamete companion cells in *Arabidopsis thaliana*

1.1 Introduction

Sexual reproduction is characterized by fertilization of an egg by a sperm cell, generating the embryo. Uniquely in angiosperms, a second sperm cell fertilizes the companion cell of the egg, the central cell, to generate the endosperm, which supports development of the embryo. During reproduction in angiosperm *Arabidopsis thaliana*, the DEMETER (DME) DNA glycosylase exhibits a striking expression pattern: Within the ovule, the female gametophyte is generated by mitosis of the haploid megaspore, forming a mature gametophyte of seven cells. During this process, the egg and central cell lineages are separated, and at this point *DME* expression is activated solely in the central cell (Park et al. 2017; Choi et al. 2002a). *DME* expression is switched off after fertilization (Choi et al. 2002a). This precise pattern of expression in the central cell, and not in the egg cell, is responsible for hypo-methylation specifically in the maternal endosperm genome and not in the maternal embryo genome (Ibarra et al. 2012). *DME*

expression in the central cell is essential for plant reproduction and genomic imprinting, whereby its absence results in loss of genomic imprinting, aberrant endosperm development and early seed abortion (Choi et al. 2002a; Gehring et al. 2006; Hsieh et al. 2011).

In the male gametophyte, indirect evidence suggests that *DME* is expressed during development of the mature 3-cell pollen grain, perhaps originating specifically in the vegetative cell, the companion cell of the two sperm cells (Schoft et al. 2011). During reproduction, the vegetative cell generates a pollen tube that transports two sperm cells to the ovule for double fertilization. While paternal inheritance of a *DME* mutation is compatible with normal seed development, it does result in decreased pollen viability and germination rates in certain ecotypes (Schoft et al. 2011; Xiao et al. 2003).

DME is required to demethylate regions of DNA as part of the base excision repair (BER) pathway. The dual activity helix-hairpin-helix glycosylase family consists of DME, REPRESSOR OF SILENCING1

(*ROS1*), DEMETER-LIKE (DML) 2 and 3. Each glycosylase enzyme acts to remove 5-methylcytosine and nick the DNA backbone, followed by repair and replacement with cytosine by downstream enzymes in the BER pathway (Gehring et al. 2006; Morales-Ruiz et al. 2006; Ortega-Galisteo et al. 2008; Gong et al. 2002). Within the glycosylase family of DNA demethylating enzymes, *DME* is distinguished by its highly restricted pattern of expression in gamete companion cells, as well as its profound effects on plant reproduction. The consequence of silencing the maternal *DME* allele is in the aberrant retention of DNA methylation on the maternal endosperm genome, including the imprinting control regions of imprinted genes (Gehring et al. 2006; Ibarra et al. 2012). Notably, maternal expression of *MEDEA* (Hilderson et al.) and *Fertilization Independent Seed 2* (*FIS2*), which form part of the floral Polycomb Repressive Complex 2 (PRC2), involved in chromatin organization and regulation, requires DME action. Without DME-mediated DNA demethylation, the expression of these genes is lost, resulting in a loss of

PRC2 and subsequent seed abortion.

DME also has a second function, which potentially impacts plant DNA methylation trans-generationally. DME-mediated DNA demethylation in companion cells is preferentially targeted to small, AT-rich, and nucleosome-depleted euchromatic transposable elements (Ibarra et al. 2012). Evidence suggests that TE hypo-methylation in the companion cells promotes transcription of mobile siRNA at the TEs, mediating RNA-directed DNA methylation (RdDM) in the gametes, so that the same TE sequences become hyper-methylated, safeguarding the genomic integrity of the gametes (Ibarra et al. 2012; Slotkin et al. 2009; Martínez et al. 2016). The large overlap between sites demethylated in the central cell, inferred from hypo-methylated sites in the maternal endosperm genome (Hsieh et al. 2009) and sites demethylated in the vegetative cell, despite their different cell fates, provides evidence towards this common basal function of *DME* expression in gamete companion cells.

Both for the appropriate expression of imprinted genes during seed development, and for the putative role of DME in transgenerational epigenetic regulation, it is vital that *DME* expression is confined to the companion cells of the gametes, and not in the gametes themselves. I therefore sought to delineate the mechanisms affording this important expression profile.

1.2 Materials and Methods

1.2.1. Plant materials and growth conditions

All the promoter constructs used in this study were transformed into *Arabidopsis* Columbia *glabrous* (Col-*gl*). The *dme-1* homozygous mutant allele is in Landsberg *erecta* (L*er*) background (Choi et al. 2002a). Heterozygous *dme-2* in Col-*gl* was used for the complementation test. *CS857766* and *SALK-036171* mutants from the ABRC stock center are Columbia 0 (Col-0) background. The plants were grown in either long-day (16hour light / 8hour dark) or short-day (8hour light / 16hour dark) photoperiodic conditions under cool white fluorescent light (100 μmole/m^2/s) at 22°C with 60% relative humidity.

1.2.2. Recombinant Plasmid Construction

The generation of the reference lines**,** *2.3kb DME::GUS* and *2.3kb DME::GFP*, were previously described (Choi et al. 2002a). All the 5' deletion constructs were generated by PCR-based cloning using a *2.3kb*

DME::GUS template in the pBI101.1 vector (Clontech Ltd.). All the *TU_GUS* lines used for fine mapping of the cis-elements were generated in the pDW137 vector (Clontech Ltd.) using the *2.3kb DME::GUS* template. Internal deletions in the *TU* lines were generated by chimeric PCR. Substitution *TU* constructs were generated by PCR-mediated site-directed mutagenesis. GUS expressions of all transgenic lines used in this study from initial independent T1 lines were summarized in Table 1-3.

1.2.3. Histochemical GUS Staining, GFP fluorescence and Microscopy

Histochemical localization of GUS activity in transgenic plants was performed on intact pistils excised longitudinally and developing stamen, incubated for 12 to 16hr at 37°C with staining solution (50mM sodium phosphate buffer, pH 7.0, 10mM potassium ferrocyanide, 10mM potassium ferricyanide, and 1mM X-gluc). GUS staining were observed with Axio Imager A1 (Carl Zeiss) microscopy. GFP fluorescence in the

gamete cells and the DAPI staining were observed with LM700 (Carl Zeiss) confocal microscopy.

1.2.4. Gene expression analysis

Total RNAs were isolated using RNA queous^{TM} (Ambion). After RNase-free DNase (TaKaRa Bio) treatment, 3ug total RNAs were used to synthesize cDNA using oligo-dT primers and M-MLV reverse transcriptase (Ambion). RNA levels were quantified by qPCR (Bio-Rad, CFX96) using iQ SYBR Green supermix (Bio-Rad) and data were analyzed with the CFX manager software (Bio-Rad). For control normalizations, I used *Actin* gene expression. My *ACT* primer set (Table 1-1) could amplify *ACT1*, *ACT3*, and *ACT12* in a single reaction. Thus, transcript levels were normalized to the total sum of *ACT1*, *ACT 3*, and *ACT 12* expression in Figure 1-1 and Figure 1-3. For the relative comparison of two *DME* splice variants (Figure 1-4), I used *ACT2* gene expression for the normalization. Relative expression levels were

quantified by the ΔΔCt method (cycle threshold (Ct) of gene of interest − cycle threshold (Ct) of the reference genes). Real-time SYBR-green dissociation curves showed one species of amplicon for each primer combination. All the primers for qRT-PCR are listed in Table 1-1.

1.2.5. Identification of DME Regulatory Regions – TUO vector series

Serial truncations of the 5'-UTR were named 'TU'. The *DME* start codon is at +639, so I amplified the region from -90 bp to +658 bp. This fragment, *TU0*, contains all the regulatory elements of endogenous DME, except the NLS. The *TU0* fragment was ligated into two different GUS-containing vectors, pBI101.1 and pDW137, to control for differences in vector efficiency. The *TU0* reporters from both vectors showed the same expression pattern and intensity as the *2.3kb DME::GUS* construct, except for GUS expression in the cytoplasm of cells expressing DME, due to the lack of an NLS in *TU0* (Figure 1-8*B* and Figure 1-10).

1.2.6. Identification of DME Regulatory Regions – Element deletion

Transgenes, *TU0_ ΔSP* (Δ+7/+45), *TU0_ ΔPOL* (Δ+416/+462), *TU0_ ΔCC1* (Δ+416/+431), *TU0_ ΔCC2* (Δ+432/+447) and *TU0_ ΔCC3* (Δ+448/+462), were generated by deleting the sequences necessary for sporophytic tissue, and central cell DME expression from *TU0* (Figure 1-14*B*). Since +472 is the end point of the 1st intron, +462 was chosen instead of +472 for the deletion to prevent potential abnormal splicing. *TU0_ΔSP* plants showed GUS expression only in the central and vegetatative cells, and *TU0_ ΔCC* and *TU0_ ΔCC3* plants showed GUS expression only in sporophytic tissues, confirming that I had successfully identified the locations of the sporophytic element (SPE) and central cell element (CCE) of the *DME* gene (Figure 1-14*A*).

1.2.7. Identification of DME Regulatory Regions – Element substitution

Transgene *TU0_ ΔHB* (Δ+450/+456) was generated by altering the known regulatory cis-element sequence in *TU0* (Figure 1-14). GUS expression of *TU0_ ΔHB* plants was not detected in vegetative cells of male gametes and was significantly reduced in central cells of female gametes.

1.2.8. Yeast one-hybrid assay

To find trans-activators that bind to the CCE, the 896 bp long -180 to +716 region was amplified and inserted into the bait vector pHIS2 (Clontech Ltd). I generated pHIS2-ΔSP2, pHIS2-ΔPOL and pHIS2-ΔCC3 constructs where, respectively, the SPE, VCE and CCE were deleted from the pHIS2-WT control construct (Figure 1-15*A*). Each construct was co-transformed, with the pGADT7 empty vector (Clontech Ltd), into the Y187 yeast strain to test the appropriate concentration of 3-amino-1,2,4-triazol (3-AT), showing that a 15mM concentration prevented self-activation. The coding

sequence of seven potential candidate DME transactivators in the central cell:.ATHB6, ATHB8, ATHB16, REV, PDF2, ANL2 and BLH7; were inserted into pGADT7 vector. For Y1H, each pHIS series and candidate construct were co-transformed into yeast strain Y187 and plated onto SD–Trp–Leu plates. 3 days after transformation, the concentration of each colony was diluted in distilled water, and then dropped onto SD–Trp–Leu plates and SD–Trp–Leu-His+3-AT(15mM) plates. Photographs were taken three days after inoculation.

1.2.9. 5' Rapid amplification of cDNA ends (5' RACE) analysis

Total RNAs extracted from Col-*gl* inflorescence using RNAqueousTM (Ambion) were treated with RNase-free DNase (TaKaRa Bio). Endogenous DME transcripts as well as the transgene transcripts were produced using 5' RACE System for Rapid Amplification of cDNA Ends, version 2.0 kit (Invitrogen) based on manufacturer's protocol. The

5’RACE products were cloned into pGEM-T Easy vector system (Promega) and sequenced

1.2.10. Bisulfite sequencing library construction.

Genomic DNA was isolated from endosperm (Hsieh et al. 2009). Paired-end bisulfite sequencing libraries for Illumina sequencing were constructed as described previously (Hsieh et al. 2009) with minor modifications. In brief, about 150 ng of genomic DNA was fragmented by sonication, end repaired and ligated to custom-synthesized methylated adapters (Eurofins MWG Operon) according to the manufacturer’s (Illumina) instructions for gDNA library construction. Adaptor-ligated libraries were subjected to two successive treatments of sodium bisulfite conversion using the EpiTect Bisulfite kit (Qiagen) as outlined in the manufacturer’s instructions. One quarter of the bisulfite-converted libraries was PCR amplified using the following conditions: 2.5 U of

ExTaq DNA polymerase (Takara Bio), 5 µl of 10X Extaq reaction buffer, 25 µM dNTPs, 1 µl Primer 1.1, 1 µl Primer 2.1 (50 µl final). PCR reactions were carried out as follows: 95ºC 3 min, then 12-14 cycles of 95ºC 30 sec, 65ºC 30 sec and 72ºC 60 sec. The enriched libraries were purified twice with solid phase reversible immobilization (Sauermann et al.) method using AM-Pure beads (Beckman Coulter) prior to quantification with a Bioanalyzer (Agilent). Sequencing on the Illumina platform was performed at the Vincent J. Coates Genomic Sequencing Laboratory at UC Berkeley and the Genome Center at UC Davis.

Table 1-1. List of primers used in this study.

Allele/Target	Name	Primer sequence
Primers for genotyping		
WT sibling of *dme-1*	B13F	5'- CTGATCAGATGCCCTTCTCC -3'
	B13R	5'- CCCAATCCATTGGTCTTGTC -3'
dme-1	B13F	5'- CTGATCAGATGCCCTTCTCC -3'
	SKI015-LB	5'- TTGACCATCATACTCATTGCTG -3'
WT sibling of *dme-2*	B33F	5'- CACTTGTTCCCTATGAGAGC -3'
	B33R	5'- CACTGATTGTGATGTTCCAC -3'
dme-2	B33R	5'- CACTGATTGTGATGTTCCAC -3'
	SKI015-LB	5'- TTGACCATCATACTCATTGCTG -3'
WT sibling of *CS857766*	-90 DME F	5'- GCAACAACGTCCTCGTGAA –3'
	+659 DME R	5'- CCGGATCAGCCCTCGAATTC -3'
CS857766	-90 DME F	5'- GCAACAACGTCCTCGTGAA –3'
	p745	5'- AACGTCCGCAATGTGTTATTAAGTTGTC -3'
WT sibling of *SALK-036171*	-90 DME F	5'- GCAACAACGTCCTCGTGAA –3'
	+659 DME R	5'- CCGGATCAGCCCTCGAATTC -3'
SALK-036171	-90 DME F	5'- GCAACAACGTCCTCGTGAA –3'
	LB3	5'-TAGCATCTGAATTTCATAACCAATCTCGATACAC -3'
Primer for RT or qRT-PCR		
DME	cDNA5	5'- CAGAAGTGTGGAGGGAAAGCGTCTGGC -3'
	SKEN5	5'- GCAATGCGTTTGCTTTCTTCCAGTCATCT -3'
ACT1 *ACT3* *ACT12*	ACT1F	5'- TCTTGATCTTGCTGGTCGTG -3'
	ACT1R	5'- AATGGTGATCACTTGCCCATC -3'
ACT2	ACT2_TAQ_F	5'- CCATCCAAGCTGTTCTCTCC -3'
	ACT2_TAQ_R	5'- GACGGAGGATGGCATGAGGAAG -3'
At5G04560.2	DME.2_TAQrpt_F	5'- CACAAGCTTGCTGAGTGGTGG -3'
	DME.2_TAQrpt_R	5'- CAGACTGACCCAACTGCTTCT C -3'
At5G04560.1	DME.1_F_TAQ	5'- GTCAATGTGAGTGATCAAATC -3'
	DME.1_R_TAQ	5'- GGTCCATCTGTTCAAAACCATG -3'

UBQ10	UBQ10-F	5’- GATCTTTGCCGGAAAACATTGGAGGATGGT -3’
	UBQ10-R	5’- CGACTTGTCATTAGAAAGAAAGAGATAACAGG -3’

1.3. Results

1.3.1. DME is Expressed Specifically in the Companion Cell of the Male Gametophyte after Separation of the Sperm Cell Lineage.

During pollen development, a haploid microspore undergoes an asymmetric mitosis to produce a bi-cellular pollen with a generative cell engulfed in the vegetative cell. A second mitosis of the generative cell generates two sperm cells (Figure 1-1*A* and *B*). Previously, a low level of *DME* transcripts had been detected in mature pollen grains but not in sperm nuclei, whilst DME-mediated DNA demethylation was shown to be restricted to the vegetative cell, implicating the vegetative cell as the site of *DME* expression (Schoft et al. 2011). However, the precise pattern of *DME* expression during male gametophyte development is unknown. To address this issue, I measured GUS and GFP reporter expression in pollen from plants bearing the previously described *2.3pDME::GUS/GFP* transgene. The *2.3pDME::GUS/GFP* construct has 2.3 kb of upstream sequence and 2 kb of the *DME* transcriptional unit fused to β-

glucuronidase (Xu et al.) or Green Fluorescent Protein (GFP), and is expressed in the central cell of the female gametophyte (Figure 1-2*A*) (Choi et al. 2002a; Kim et al. 2008). GUS or GFP reporter expression was only detected in the vegetative cell nucleus of late bi-cellular pollen; that is, after the first asymmetric mitosis, but not in the generative or sperm cell nuclei, or at any other stages of pollen development (Figure 1-1*A*, lower panel and *B*). qRT-PCR analysis was in accord with these results, showing elevated *DME* RNA expression at the bi-cellular pollen stage followed by rapid decreases as pollen matured (Figure 1-1*C*). Thus, *DME* expression is not detected until the sperm cell lineage is separated from that of the vegetative cell, at which point DME is active specifically in the vegetative cell.

Figure 1-1.

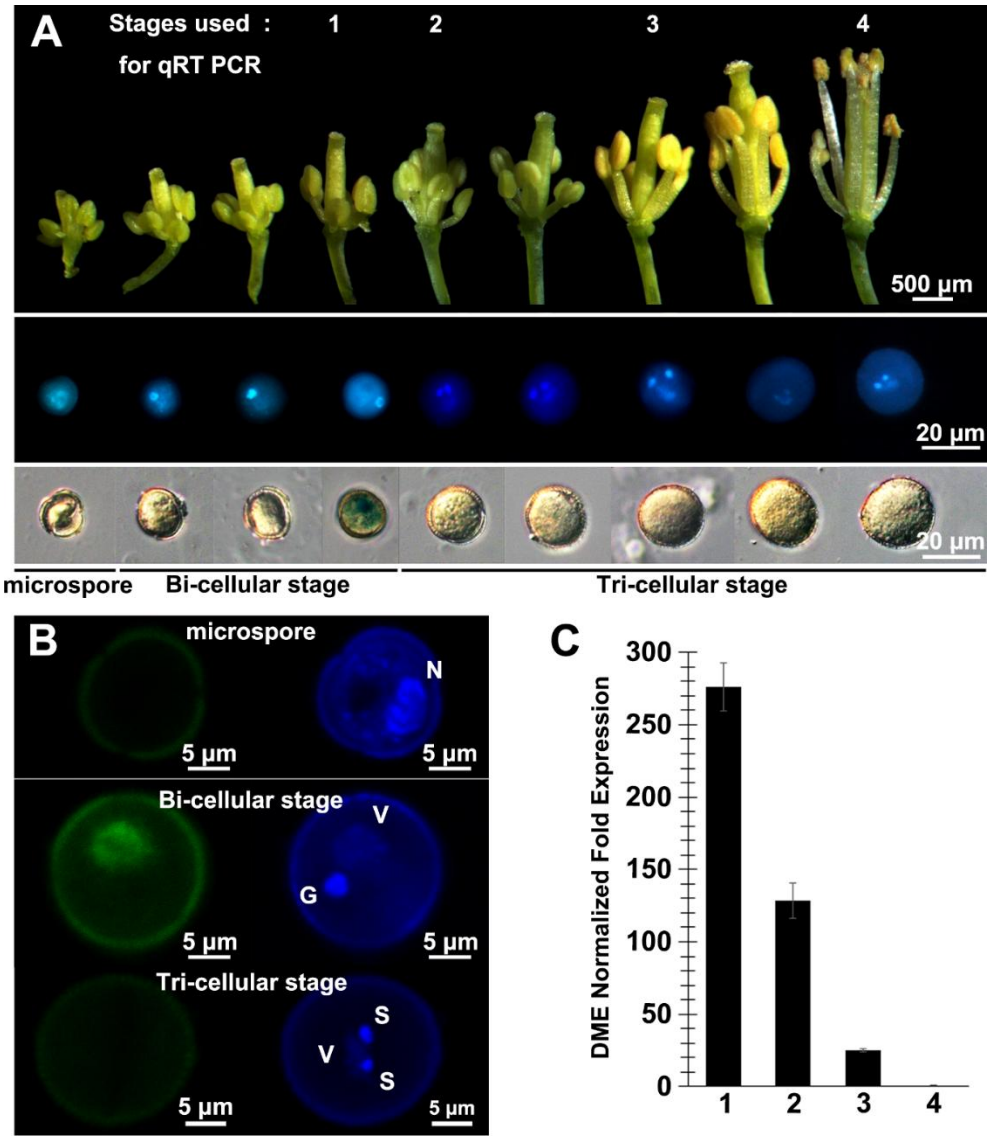

Figure 1-1. *DME* is specifically expressed in the vegetative nucleus of late bi-cellular stage pollen.

(*A*) Sequential development of flowers (Merkley et al.) and corresponding pollen development in *2.3 kb DME::GUS* transgenic plants with DAPI (middle) and GUS staining (bottom). (*B*) *2.3 kb DME::GFP* expression

(left) in microspore (Merkley et al.), bi-cellular (middle) and tri-cellular (bottom) stage pollen grains stained with DAPI (Wong et al.). N, microspore nucleus; G, generative nucleus; V, vegetative nucleus; S, sperm cell nucleus; Scale bars = 5μm. (*C*) qRT-PCR analysis of DME expression in wild-type pollen development after normalization with *ACT1*, *ACT3*, and *ACT12* expression. The four different stages analyzed using qRT-PCR are indicated in (*A*). Values are plotted relative to the expression of DME in stage 4 mature pollen which was set at 1.0, and represent the average of triplicate measurements ± standard deviation.

Figure 1-2.

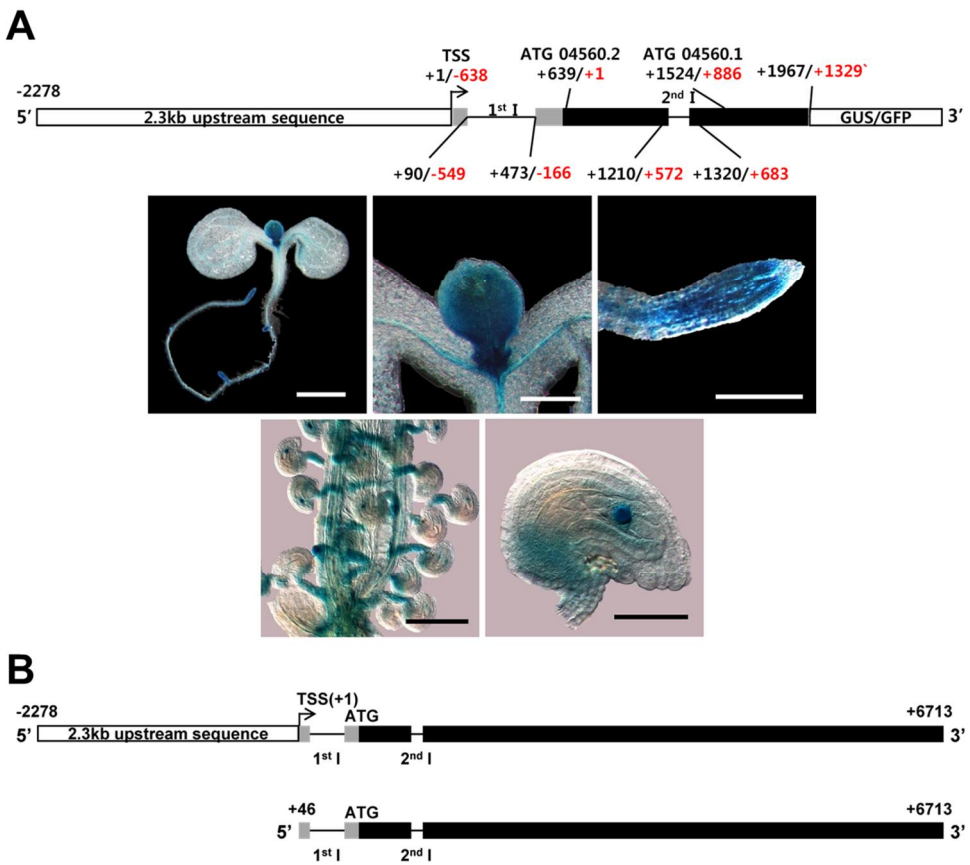

Figure 1-2. Diagram and expression of a *2.3 kb DME::GUS* reference line and two complementing constructs.

(*A*) Diagram (top section) and expression pattern (middle and bottom sections) of a *2.3 kb DME::GUS* reference line. The number in black before the slash is based on a new TSS that I defined using 5' RACE (see Figure 1-4). The number in red after the slash is based on the translation start site of At5g04560.2, the major splice variant. The middle section

shows images of seedlings at 7 days after germination (DAG 7), showing shoot meristems on the left and root tips on the right. The bottom section shows pistils on the left and an ovule at higher magnification on the right. (*B*) Diagram of the two c*DME* complementation constructs with 2.3 kb upstream sequences (2.3 kb *cDME*) or deleted 5' UTR (+46 *cDME*). Both constructs contain the 1st and 2nd introns.

1.3.2. The DME Promoter Lies within the DME Transcriptional Unit and Contains Both Positive and Negative Regulatory Elements.

In order to identify the elements that promote the striking pattern of *DME* expression in male and female companion cells, I systematically deleted portions of my *2.3pDME::GUS* reference construct (Figure 1-3*A*). Deletion of the entire 5' region, from -2.3 kb to +46 bp downstream of the transcriptional start site (Rud et al.), as defined by 5' RACE, (Figure 1-3*A*, *B* and Figure 1-4), had no effect on *DME::GUS* expression in the central and vegetative cells. For each of these deletion constructs, both temporal and spatial *DME::GUS* expression profiles in transgenic plants reflected those of the reference construct (Figure 1-2*A*, 1-3*A* and *B*). I then deleted a larger block of sequence, up to 395 bp downstream of the TSS, at which point *DME* expression was decreased, and finally, deletion of *DME* transcriptional unit sequence to 473 bp downstream of the TSS led to the complete loss of *DME::GUS* expression in both central and vegetative cells (Figure 1-3*A* and *B*). These data indicate the presence of regulatory

sequences that are required for the proper expression of DME in the central and vegetative cells lie between 46 and 473 bp downstream of the TSS.

To verify genetically that DNA sequences upstream of the TSS do not regulate DME expression, I obtained two T-DNA insertion mutants from the Arabidopsis Biological Resource Center: *CS857766,* which has a T-DNA insertion 72 bp upstream (-72) of the TSS, and *SALK -036171,* which has a T-DNA insertion 25 bp upstream (-25) of the TSS (Figure 1-3*C*). Homozygous mutants of either line were developmentally and morphologically indistinguishable from wild type and did not exhibit any defects in fertility or seed viability (Table 1-2), suggesting that *DME* is appropriately expressed and functions normally in these mutants. *DME* is also expressed in sporophyte tissues (Kim et al. 2008), and I found the level of *DME* expression in homozygous *CS857766* and *SALK-036171* seedlings to be the same as in wild-type seedlings (Figure 1-3*D*).

In transgenic plants where the sequence downstream from +83 was

deleted and the upstream portion fused to GUS directly, '*2.3kb Pro DME::GUS'*, GUS expression was absent from the central and vegetative cells (Figure 1-3*A* and *B*; central cell nucleus within ovule indicated with arrow). However, strong ectopic GUS activity was observed in the synergid cells of mature female gametophytes in plants expressing this transgene (Figure 1-3*A* and *B,* arrowhead, and Table 1-3). Thus, a putative suppressor element that usually represses *DME* expression in synergid cells is present downstream of +83 bp. The lack of an NLS in this construct resulted in staining of the synergid cells' cytoplasm.

Figure 1-3.

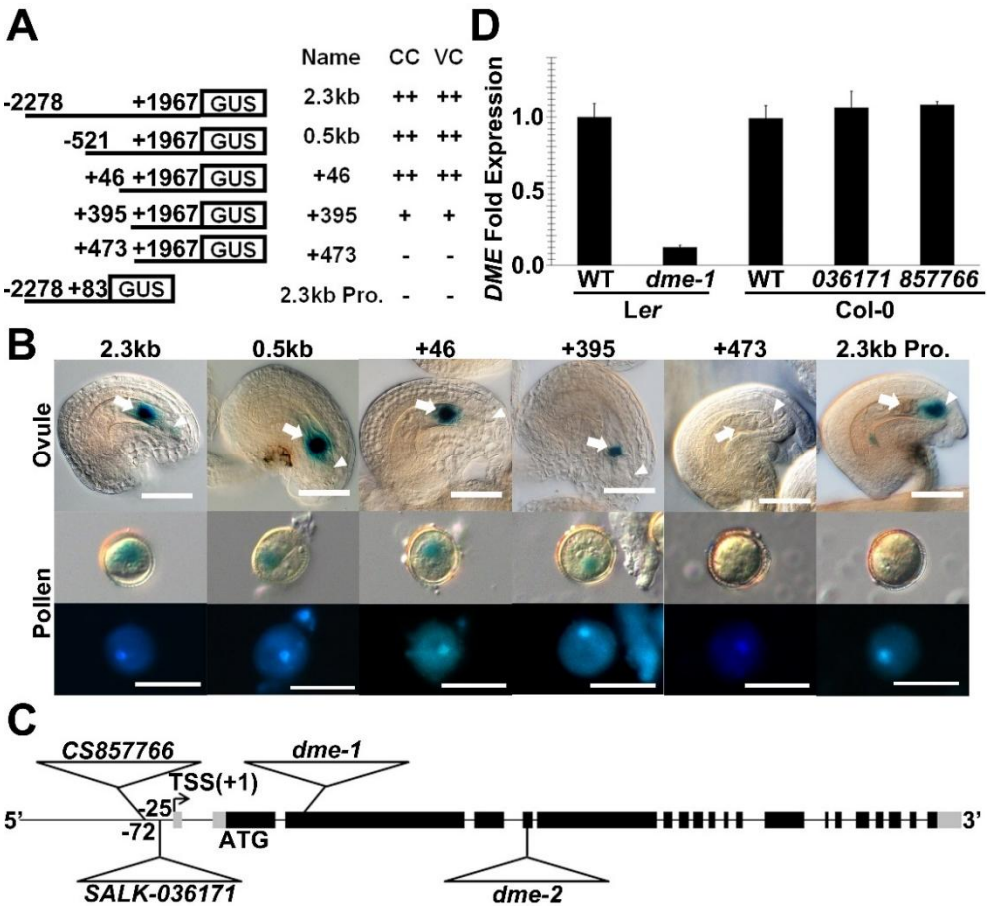

Figure 1-3. Diagram of the *DME::GUS* reporter constructs and expression of the T-DNA insertion lines in the *DME* region.

(*A*) The name, staining intensity and the coordinates for each construct are shown. CC, central cells; VC, vegetative cell of pollen; [-, none; +, moderate; ++, strong]. (*B*) GUS staining is shown in ovules and pollen. DAPI-stained pollen grains are shown in the bottom row. Plants

expressing transgenes 2.3kb to +395 displayed GUS expression in the central cell nucleus (arrow) and vegetative cell nucleus. No GUS expression was detected in +473 transgenic plants and 2.3kb Pro. plants exhibited GUS expression only in the synergid cells (arrowhead). Scale bars = 50μm in ovule, 20μm in pollen. (*C*) *dme* T-DNA insertion alleles at 72 nt upstream (*CS857766*) and at 25 nt upstream (*SALK-036171*) of the TSS. Black box, translated exon; gray box, untranslated exon; first line, 5' flanking sequences; other lines, intron. (*D*) qRT-PCR analysis of *DME* expression in homozygous *dme* mutant seedlings after normalization with *ACT1*, *ACT3*, and *ACT12* expression. Values are plotted relative to the expression of *DME* in L*er* wild type which was set at 1.0, and represent the average of triplicate measurements ± standard deviation.

Figure 1-4.

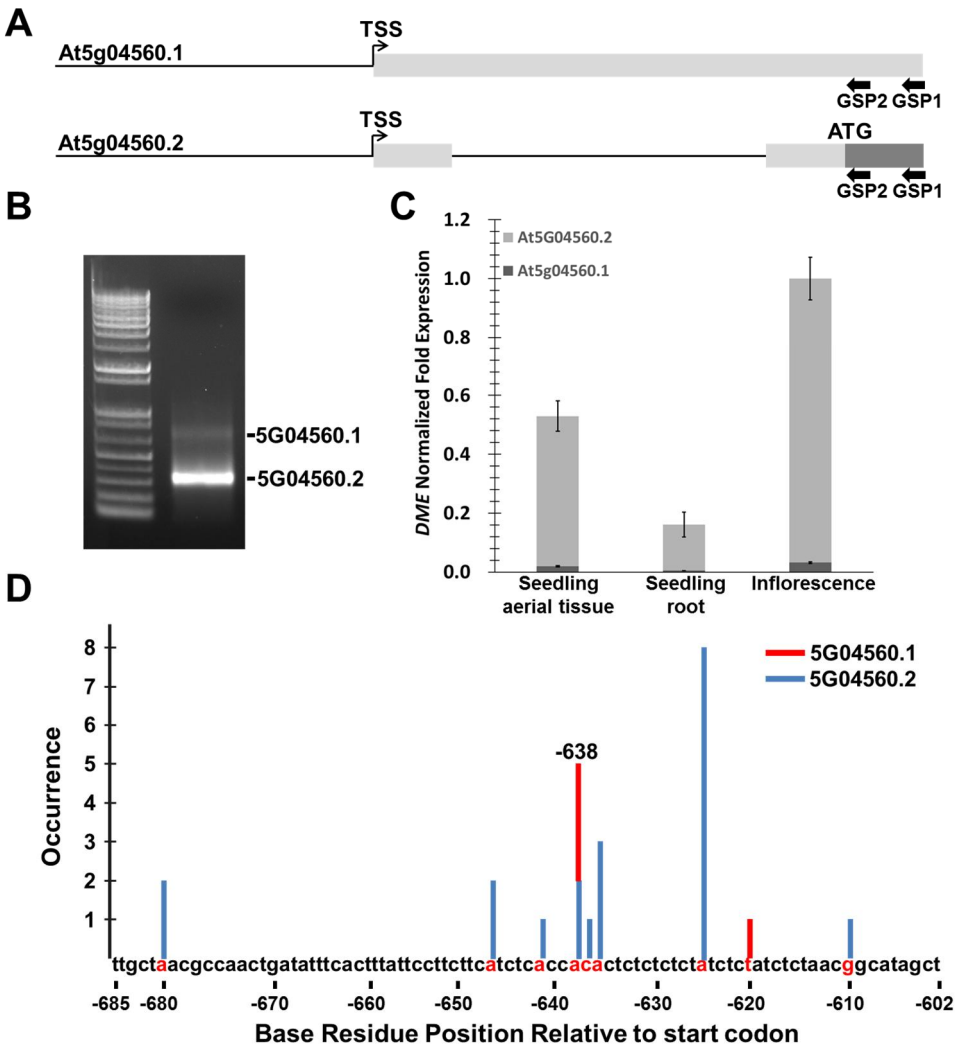

Figure 1-4. 5' RACE analysis of *DME* using inflorescence RNA.

(*A*) Diagram of the two alternative forms of the *DME* 5' region. Light gray box, 5'-UTR; dark gray box, translated exon; front line, 5'flanking region; second line, 1st intron; black arrow, 5' RACE primer; TSS, transcription

start site; GSP, gene-specific primer. (*B*) Agarose gel electrophoresis of *DME* 5′ RACE products from total inflorescence RNA using the GSP2 primer. (*C*) qRT-PCR analysis to compare the relative expression levels of the two *DME* splice variants, *At5g04560.1* and *At5g04560.2,* in aerial tissue and root tissue of two-week old seedling and in immature inflorescences. Expression levels are normalized to the *ACT2* housekeeping gene and represent the average of triplicate measurements standard deviation. (*D*) Relative distribution of *DME* TSS determined by 5' RACE clones. Nucleotide positions relative to the start codon are indicated on the X-axis. The graph summarizes the results of 24 RACE clones.

Table 1-2. Seed abortion in *dme* alleles.

Genotype	Number of siliques	Total Viable seed	Total Aborted seed	Average seed abortion ratio (%) ± SD
Col-*gl*	8	374	0	0
CS857766/ *CS857766*	6	321	1	0.3 ± 0.7
SALK-036171/ *SALK-036171*	6	348	1	0.3 ± 0.7
DME/*dme-2*	9	181	185	50.5 ± 9.5

Table 1-3. Expression of T1 pDME:GUS transgenic plants, listing the number, with the proportion in parentheses, of lines that exhibited positive GUS expression

Construct	Sporophytic(/Total)	Central cell(/Total)	Vegetative cell(/Total)	Total
2.3kb	14(0.74)	18(0.95)	18(0.95)	19
0.5kb	8(0.80)	10(1)	10(1)	10
+7	9(1)	9(1)	9(1)	9
+20	0(0)	18(0.95)	18(0.95)	19
+33	5(0.29)	17(1)	17(1)	17
+46	0(0)	22(1)	22(1)	22
+395	0(0)	17(1)	14(0.82)	17
+473	0(0)	0(0)	0(0)	13
2.3kb Δ5'	18(0.90)	20(1)	20(1)	20
2.3kb Pro.	13(0.72)	0(0)	0(0)	18
TU0	12(1)	11(0.92)	11(0.92)	12
TU12	5(0.50)	0(0)	0(0)	10
TU13	14(0.82)	0(0)	0(0)	17
TU14	6(0.55)	9(0.82)	9(0.82)	11
TU23	0(0)	0(0)	0(0)	15
TU24	0(0)	14(0.88)	14(0.88)	16
TU25	2(0.17)	12(1)	12(1)	12
TU34	1(0.08)	10(0.83)	10(0.83)	12
TU35	1(0.11)	9(1)	9(1)	9
TU45	0(0)	10(0.67)	9(0.60)	15
TU0_ΔSP	3(0.20)	14(0.93)	14(0.93)	15
TU0_ΔPOL	10(0.67)	4(0.27)	3(0.20)	15
TU0_ΔCC1	15(1)	11(0.73)	11(0.73)	15
TU0_ΔCC2	20(1)	20(1)	20(1)	20
TU0_ΔCC3	14(0.93)	4(0.27)	4(0.27)	15
TU0_ΔHB	6(0.55)	2(0.18)	2(0.18)	11

1.3.3. Expressing DME Polypeptide in the Central Cell with a Minimal Reproductive Promoter Rescues Seed Abortion and Aberrant DNA methylation associated with the *dme-2* mutation.

The *+46 pDME::GUS/GFP* transgene has the shortest sequence that correctly regulates reporter expression in the central cell and vegetative cells, without deleting internal DME coding sequences (Figure 1-3*A*, *B* and Figure 1-5*A*). I therefore considered this transgene to contain the minimal reproductive promoter that could be used to drive the correct reproductive expression of a full-length DME polypeptide in a functional assay. I then constructed a *+46 pDME::cDME* transgene (Figure 1-2*B*) to determine the functional significance of *DME* expression driven by this minimal reproductive promoter. I transformed *dme-2* heterozygotes with the *+46 pDME::cDME* transgene (Figure 1-5*B*)**.** The *dme-2* mutation is a loss-of-function null allele, and in self-pollinated *dme-2* heterozygous mutant plants, 50% of the F1 progeny seed inherit the maternal *dme-2* mutant allele and abort their development, whilst inheritance of the

paternal mutant *dme-2* allele has no effect on seed viability (Choi et al. 2002a). To test for *+46 pDME::cDME* transgene function, I analyzed whether it could rescue seed abortion in transgenic lines. In self-pollinated plants that were hemizygous for a single transgene locus, and heterozygous for *dme-2*, 25% of the F1 seed inherit the mutant maternal *dme-2* allele and abort their development, and 25% inherit both the mutant maternal *dme-2* allele and the transgene. Hence, full complementation of the mutant maternal *dme-2* allele by the *+46 pDME::cDME* transgene results in 25% seed abortion (Choi et al. 2002a), which I observed (Figure 1-5*B* and Table 1-4). Moreover, self-pollination of plants heterozygous for *dme-2* and hemizygous for *+46 pDME::cDME* generated plants homozygous for both the *dme-2* mutation and the *+46 pDME::cDME* transgene, which displayed the same low seed abortion rate (<1 %) as both wild-type plants and homozygous *dme-2* plants expressing the homozygous *2.3kb pDME::cDME* control transgene (Figure 1-5 and Table 1-4), demonstrating the functional activity of the minimal reproductive

promoter.

Seed abortion resulting from the *dme-2* mutation is caused, at least in part, by the resultant aberrant expression pattern of imprinted components of the PRC2 in endosperm (Grossniklaus et al. 1998; Kohler et al. 2003; Choi et al. 2002a; Gehring et al. 2006; Luo et al. 2000). In the absence of DME, PRC2 is defective, and endosperm development is severely compromised, resulting in embryo abortion (Hehenberger, Kradolfer, and Kohler 2012). Since seed abortion is rescued by the *+46 pDME::cDME* transgene, I hypothesize that *DME* expression driven by the minimal reproductive promoter is able to demethylate the central cell genome-wide, including specific PRC2 genes, resulting in a functional endosperm with a distinctive pattern of maternal endosperm genome hypomethylation compared to the paternal endosperm genome. To test this hypothesis, I pollinated *dme-2/dme-2* homozygous Col-*gl* (Columbia ecotype, homozygous for the *glabrous* mutation) plants that were also homozygous for the *+46 pDME::cDME* transgene, with wild-type L*er*

(Landsberg ecotype homozygous for the *erecta* mutation) pollen. F1 seeds were harvested at 9 days after pollination, endosperm was obtained by manual seed dissection, and genomic DNA was isolated. Maternal and paternal genomes were distinguished by Col versus L*er* single nucleotide polymorphisms, and DNA methylation profiles were obtained by next generation bisulfite sequencing of DNA (Ibarra et al. 2012). I analyzed the methylome of F1 endosperm from *dme-2/dme-2* homozygotes that were homozygous for the *+46 pDME::cDME* transgene (*dme-2*; *+46 cDME*), and compared it to a wild-type control (Col-0 crossed to L*er*), and to the methylome of seeds inheriting the *dme-2* mutation maternally (Ibarra et al. 2012). I found that the maternal allele of F1 *dme-2*; *+46 cDME* endosperm is normally methylated at maternally (e.g. *FIS2, FWA*) and paternally (e.g. *YUK10, PHE1*) expressed imprinted gene loci, and resembles the wild type maternal allele, whereas these loci are hypermethylated in *dme-2* (Figure 1-6). Genome-wide, the hypermethylation phenotype seen in *dme-2* maternal endosperm, demonstrated by the increased density of genomic

sites with a fractional methylation level between 0.5 and 1 (Figure 1-6*B*, *dme-2* minus wild type kernel density trace), is fully complemented in *dme-2*; *+46 cDME* endosperm, and resembles the wild-type endosperm methylome (Figure 1-6*B*, *dme-2*; *+46 cDME* minus wild type trace; Figure 1-7), whereas the paternal allele is unaffected (Figure 1-6*C*). Thus, the minimal reproductive promoter promotes functional *DME* expression required for DNA demethylation.

Figure 1-5.

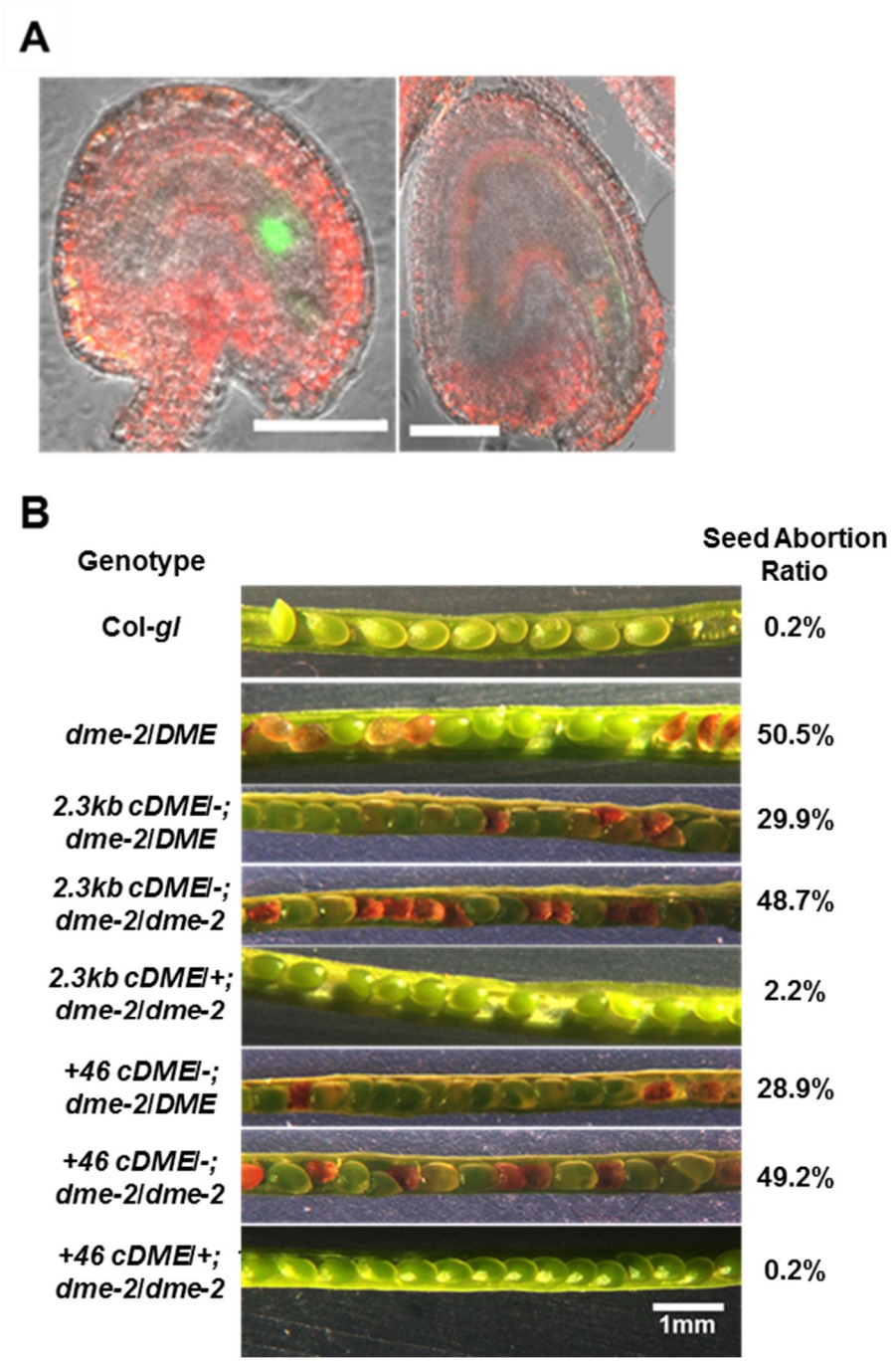
A
B
Genotype
Seed Abortion Ratio
Col-gl
0.2%
dme-2/DME
50.5%
2.3kb cDME/-; dme-2/DME
29.9%
2.3kb cDME/-; dme-2/dme-2
48.7%
2.3kb cDME/+; dme-2/dme-2
2.2%
+46 cDME/-; dme-2/DME
28.9%
+46 cDME/-; dme-2/dme-2
49.2%
+46 cDME/+; dme-2/dme-2
0.2%
1mm

Figure 1-5. DME expression driven by the +46 minimal reproductive promoter transgene rescues *dme-2*-mediated seed abortion.

(*A*) The +46 *pDME:GFP* transgene is expressed in the central cell before fertilization, but not in the endosperm after fertilization. Scale bars = 50μm. (*B*) Siliques of *dme-2* mutants containing *2.3kb cDME* or *+46 cDME* complementing constructs. See also Figure 1-2 and Table 1-4. Scale bar = 1mm

Figure 1-6

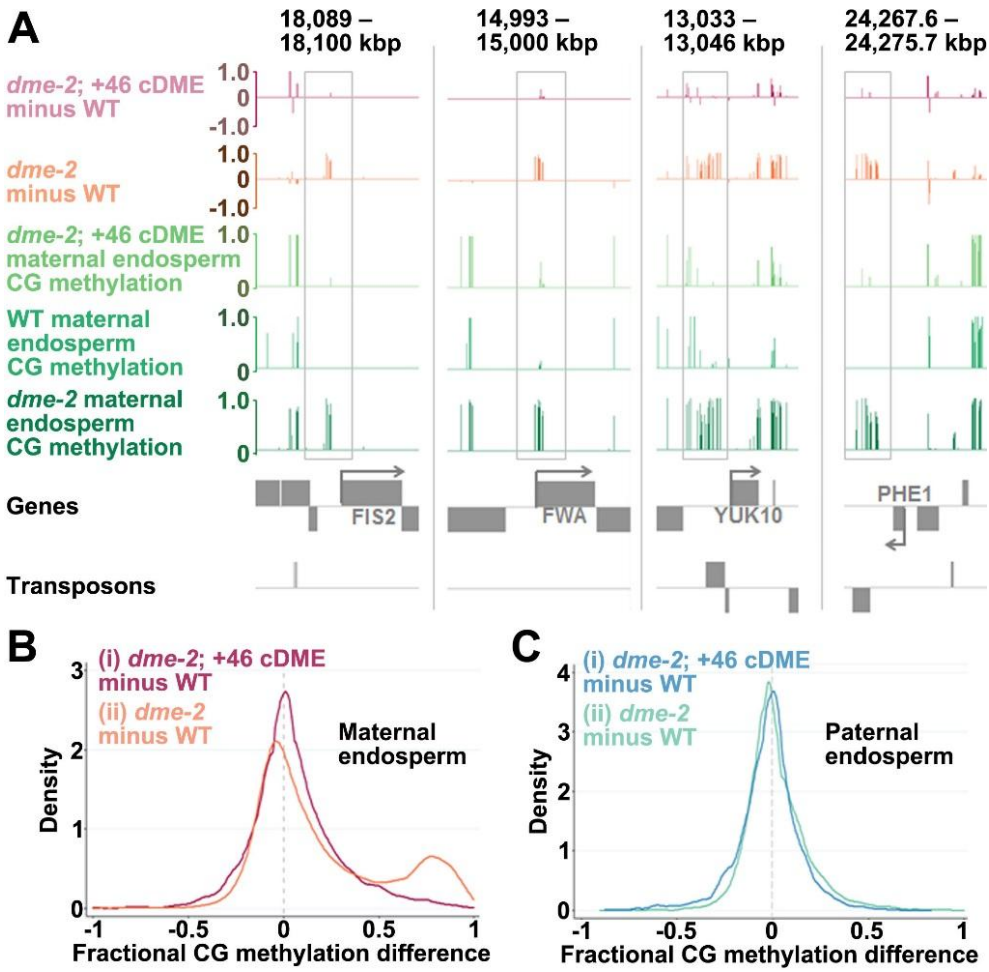

Figure 1-6. *DME* expression driven by the +46 transgene can correct the methylation phenotype of homozygous *dme-2* mutant endosperm.

(*A*) Snap shots of CG DNA methylation at selected imprinted loci. Each track represents a different genotype: Crimson trace, WT subtracted from *dme-2* homozygous endosperm expressing the +46 transgene; Orange

trace, WT subtracted from *dme-2* heterozygous endosperm; Green tracks are raw CG methylation data in the three genotypes compared. Differential methylation at both maternally expressed (*FIS2, FWA*) and paternally expressed (*YUK10, PHE1*) imprinted loci, i.e. maternal hypomethylation of imprinting control regions, is regained in *dme-2* homozygous endosperm when the +46 transgene is expressed. Grey boxes show the imprinting control regions at each locus and arrows show the direction of gene transcription. (*B*) Kernel density plots of CG methylation differences between the maternal alleles of (i) Crimson trace, *dme-2* homozygous endosperm expressing the +46 transgene and wildtype and (Niki et al.) orange trace, *dme-2* heterozygous endosperm and wildtype. Hypermethylation of the *dme-2* mutant endosperm is evident in the increased density at a fractional methylation difference of between 0.5 and 1 in (Niki et al.), and is corrected by the +46 transgene as seen by the loss of this density increase in (i). (*C*) Kernel density plots of CG methylation differences between the paternal alleles of (i) Blue trace, *dme-2*

homozygous endosperm expressing the +46 transgene, and wild type and (Niki et al.) aquamarine trace, *dme-2* heterozygous endosperm and wild type. Methylation of the paternal (wild type Landsberg) alleles is the same in each genotype, showing that the +46 transgene does not affect methylation post-fertilization.

Figure 1-7

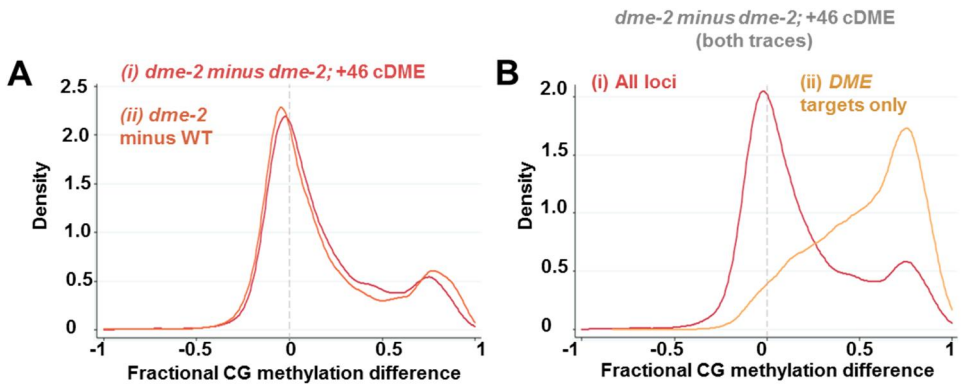

Figure 1-7. DME expression driven by the +46 minimal reproductive promoter transgene can correct the methylation phenotype of homozygous *dme-2* mutant endosperm.

(*A*) Kernel density plots of CG methylation differences between the maternal alleles of (i) red trace, *dme-2* mutant endosperm (Ibarra et al. 2012) and *dme-2* mutant endosperm expressing the +46 transgene. (Niki et al.) orange trace, *dme-2* heterozygous endosperm and wildtype. Similar hypermethylation of the *dme-2* mutant endosperm relative to both the WT and the *dme-2* mutant expressing the +46 transgene is evident in the increased density at a fractional methylation difference of between 0.5 and 1 in both plots. Compared to the *dme-2* mutant endosperm, the same genomic sites are relatively hypomethylated in WT and the +46 transgene

DNA. (*B*) Kernel density plots of CG methylation differences between the maternal alleles of *dme-2* mutant endosperm and *dme-2* mutant endosperm expressing the +46 transgene for (i) all genomic sites (Niki et al.) DME target sites only

Table 1-4. Seed abortion ratio of *dme-2* mutants containing two different complementing constructs

Genotype	Total viable seed	Total aborted seed	Average seed abortion ratio (%) ± SD	χ2	P
Col-*gl*	434	1	0.2 ± 0.6		
2.3kb cDME/- ; *DME*/*dme-2* F1	344	147	29.9 ± 5.9	0.0114 (3:1)	>0.90 (3:1)
+46 cDME/- ; *DME*/*dme-2* F1	324	132	28.9 ± 5.2	0.0516 (3:1)	>0.80 (3:1)
2.3kb cDME/- ; *dme-2*/*dme-2* F2	286	271	48.7 ± 6.7	0.5251 (1:1)	>0.45 (1:1)
2.3kb cDME/ *2.3kb cDME* ; *dme-2*/*dme-2* F2	264	6	2.2 ± 3.5		
+46 cDME/- ; *dme-2*/*dme-2* F2	189	183	49.2 ± 5.2	0.7557 (1:1)	>0.35 (1:1)
+46 cDME/ *+46 cDME* ; *dme-2*/*dme-2* F2	552	1	0.2 ± 0.5		
DME/*dme-2*	142	145	50.5 ± 9.5	0.8594 (1:1)	>0.35 (1:1)

Table 1-4. Seed abortion ratio of *dme-2* mutants containing two different complementing constructs.

I selected heterozygous *dme-2* mutants with single copy transgenes using the antibiotic resistant ratio: for the *2.3kb cDME* control promoter transgene I observed an 81 : 17 resistant : sensitive ratio. For the *+46 cDME* minimal reproductive promoter transgene, I observed a 95 : 22 ; resistant : sensitive ratio. I detected a significant reduction in seed abortion, 28.9 % (N = 456) with the *+46 cDME* minimal reproductive promoter transgene, compared to 50.5% seed abortion (N = 287) in *dme-2/DME* control plants. Similar observations of 29.9% seed abortion (N = 491) were obtained using the control 2.3 kb *DME* promoter. This indicates that expressing the DME polypeptide using the minimal reproductive promoter is sufficient to complement seed abortion caused by the *dme-2* loss-of-function mutation. P, Probability that the deviation from the indicated segregation ratio of viable : aborted seeds is due to chance. See also Figure 1-4 and 1-5*B*.

1.3.4. A 357 bp Region of the *DME* Transcriptional Unit is both Necessary and Sufficient to Generate the Appropriate *DME* Expression Profile during Female Gametophyte Development.

To identify where the precise regulatory elements that control DME expression in the central cell are located, I carried out further deletions within the 2 kb region that I had so far identified to be necessary and sufficient for fully functional DME activity. This Gain-of-Function (GOF) construct series is denoted 'Truncated 5'-UTR' (Drews and Koltunow) (Figure 1-8*A* and Figure 1-9), for which I used increasingly smaller portions of the 748 bp long -90 to +658 region around the DME TSS to drive GUS expression. The *TU0* reporter construct, containing the full -90 to +658 region, showed the same expression pattern and intensity as the reference *2.3pDME::GUS* construct, except for GUS expression in the cytoplasm of cells expressing GUS since the endogenous nuclear localization sequence of DME is downstream of 658 bp, and therefore absent from all TU constructs (Figure 1-8*A*, *B*, Figure 1-9 and 1-10).

From my GOF TU series, the minimal sequence that I found to be necessary and sufficient to drive *DME* expression in the central cell was 357 bp in length, from +202/+559 (transgene TU34, Figure 1-8*A* and *B*). *TU23* (+46/+415) plants did not show any GUS expression, but *TU34* plants displayed GUS activity in the central cell (Figure 1-8*A* and *B*). Since my previous deletion to 473 bp downstream of the TSS led to the complete loss of DME::GUS expression (Figure 1-3*A*), I deduced that the central cell regulatory region lies in a 57 bp fragment between the +416 and +472 positions. I also observed reduced GUS expression in the central cell in *TU45* (+363/+658), indicating that quantitative regulation of central cell expression also involves a region between +202 and +362, denoted the quantitative regulatory element (QE).

The *TU23, TU24, TU25, TU34, TU35* and *TU45* transgenes do not include the *DME* TSS sequence (Figure 1-8 and Figure 1-9). I was therefore intrigued to identify where the transcripts began. 5' RACE was performed on total RNAs from *TU0* (which includes the endogenous TSS

sequence), *TU25* and *TU35* inflorescences. The TSS for all transgenes, regardless of whether the sequence was endogenous or part of the vector, was consistently several hundred bases upstream of the enhancer elements (Figure 1-11*A*). Splicing between the vector and the 3'end of *DME*'s first intron occurred normally (Figure 1-11*A*). I compared the DNA sequence around the TSS of endogenous *DME* and that of the *TU25* and *TU35* vector regions but did not find any striking sequence motifs (Figure 1-11*B*).

Figure 1-8.

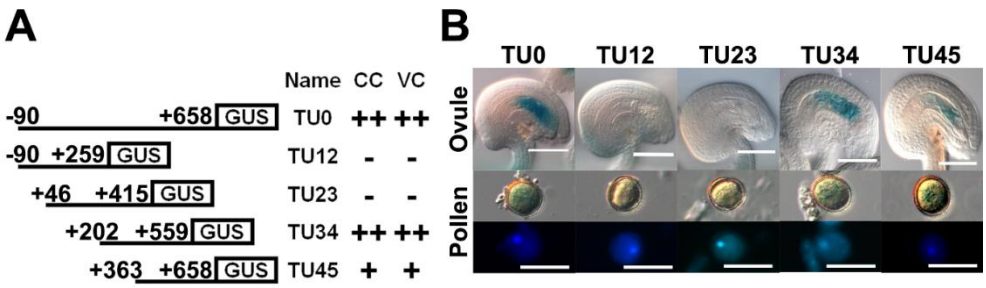

Figure 1-8. Diagram of the *DME::GUS* reporter constructs for fine mapping of cis-elements and their expression patterns.

The TU (truncated 5'-UTR) series of constructs. (*A*) The name, staining intensity and coordinates for each construct are shown. CC, central cells; VC, vegetative cell of pollen; [-, none; +, moderate; ++, strong]. (*B*) GUS staining is shown in ovules and pollen. DAPI-stained pollen grains are shown in the bottom row. TU0, TU34 and TU45 transgenic plants exhibited GUS expression in the central cell and pollen. No GUS expression was detected in TU12 and TU23 plants. Scale bars = 50μm.

Figure 1-9.

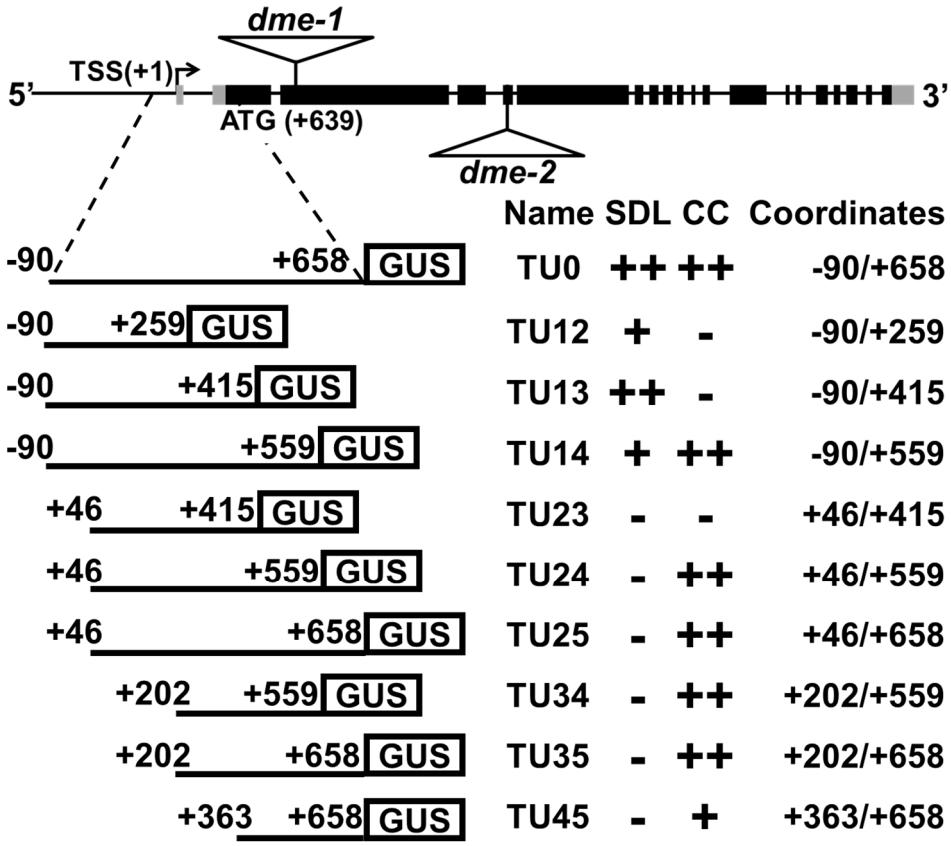

Figure 1-9. Diagram of the *DME::GUS* reporter constructs for fine mapping of cis-elements.

The TU (truncated 5'-UTR) series of constructs. The name, staining intensity and the coordinates for each construct are shown. SDL, seedling; CC, central cells; [-, none; +, moderate; ++, strong].

Figure 1-10.

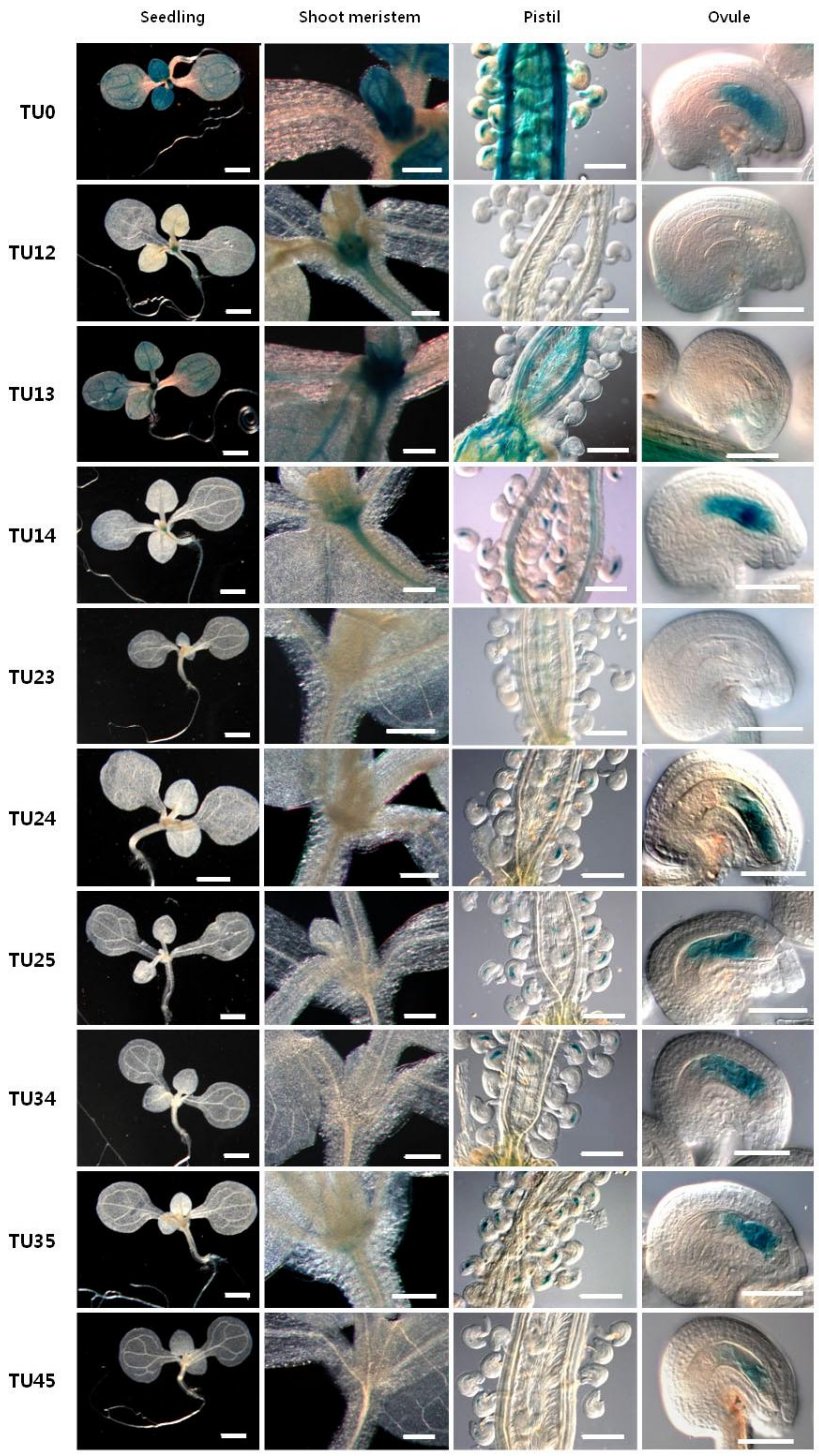
Seedling
Shoot meristem
Pistil
Ovule
TU0
TU12
TU13
TU14
TU23
TU24
TU25
TU34
TU35
TU45

Figure 1-10. Catalog of the Expression Patterns of the TU DME:GUS Construct Series.

TU12, *TU13*, and *TU23* plants showed weak GUS signal only in sporophytic tissues. By contrast, *TU34*, *TU35*, and *TU45* plants showed GUS expression only in central cells. Scale bars = 1000μm in seedlings, 200μm in shoot meristem and pistil, 50μm in ovule.

Figure 1-11.

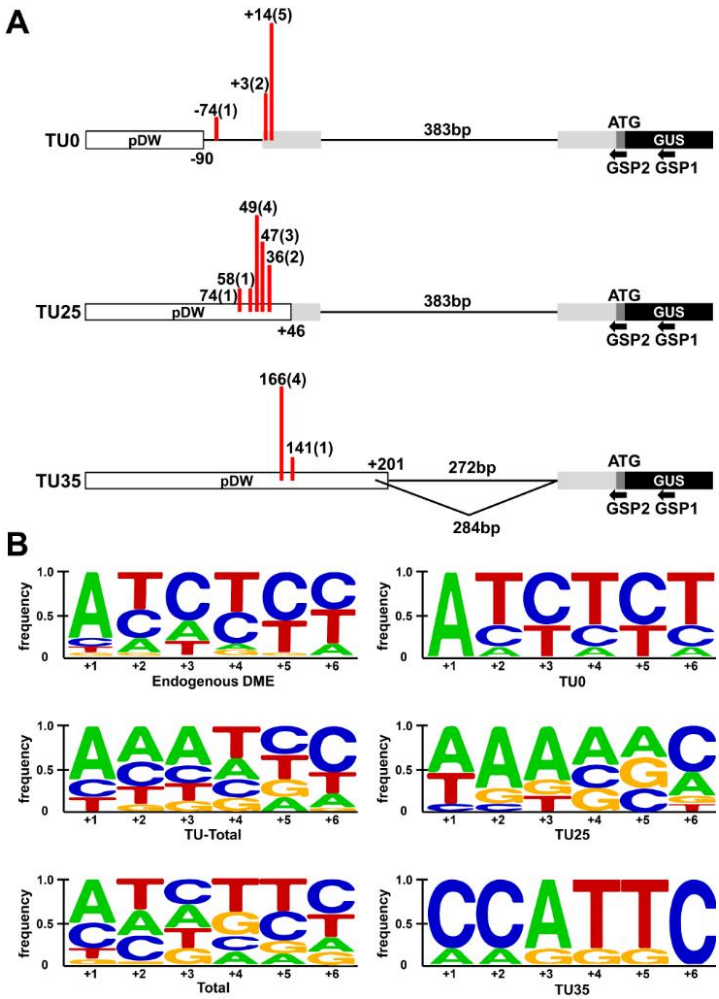

Figure 1-11. Identification of the TSS of the TU transgenes.

(*A*) Relative distribution of TSSs of the TU transgenes determined by 5'-RACE using inflorescence RNA. Number points to the 5'end of transgene transcripts (*TU0*; relative to TSS of *DME*, *TU25* and *TU35*; length of vector sequence in the transcripts). Number of clones obtained within

parenthesis.

(*B*) Sequence LOGOs of TSS-flanking sequences in the endogenous *DME* gene and three transgenes, *TU0*, *TU25* and *TU35*. The 6 bp after each TSS were analyzed using WebLogo (http://weblogo.berkeley.edu/) (Schneider and Stephens 1990; Crooks et al. 2004). The "Endogenous DME" LOGO output was derived from all 24 5' RACE products shown in Figure 2-4*D*. the "TU-Total" LOGO was derived from all three transgenes and "Total" LOGO was from all 5' RACE products of endogenous *DME,* as well as from the three transgenes.

1.3.5. *DME* Expression in Sporophytic Tissues Is Regulated by Distinct DNA Sequences.

DME is expressed in the sporophyte shoot apical meristem (SAM), leaf primordia, and the root apical meristem (Figure 1-2*A*, 1-9, 1-10, 1-12, 1-13) and is required for floral and vegetative developmental patterning (Choi et al. 2002a; Kim et al. 2008). To determine the relationship between the regulation of *DME* in reproductive and sporophytic tissues, I further investigated the regulatory regions of *DME* to elucidate those required for sporophytic *DME* expression. I identified a 349 bp region, from -90 to +259 that is necessary and sufficient for *DME* expression in sporophytic tissues (TU12, Figure 1-9 and 1-10). Next, I generated constructs to narrow this region, identifying 13 bp close to the TSS, between +7 and +19, required for the sporophytic expression of DME, which I designate as a necessary sporophytic enhancer, SPE (Figure 1-12, 1-13 and 1-14*A*). Deletion specifically of the SPE, (*TU0_ΔSP)* results in loss of sporophytic, but not reproductive, DME expression (Figure 1-14*B*

and *C*).

Figure 1-12.

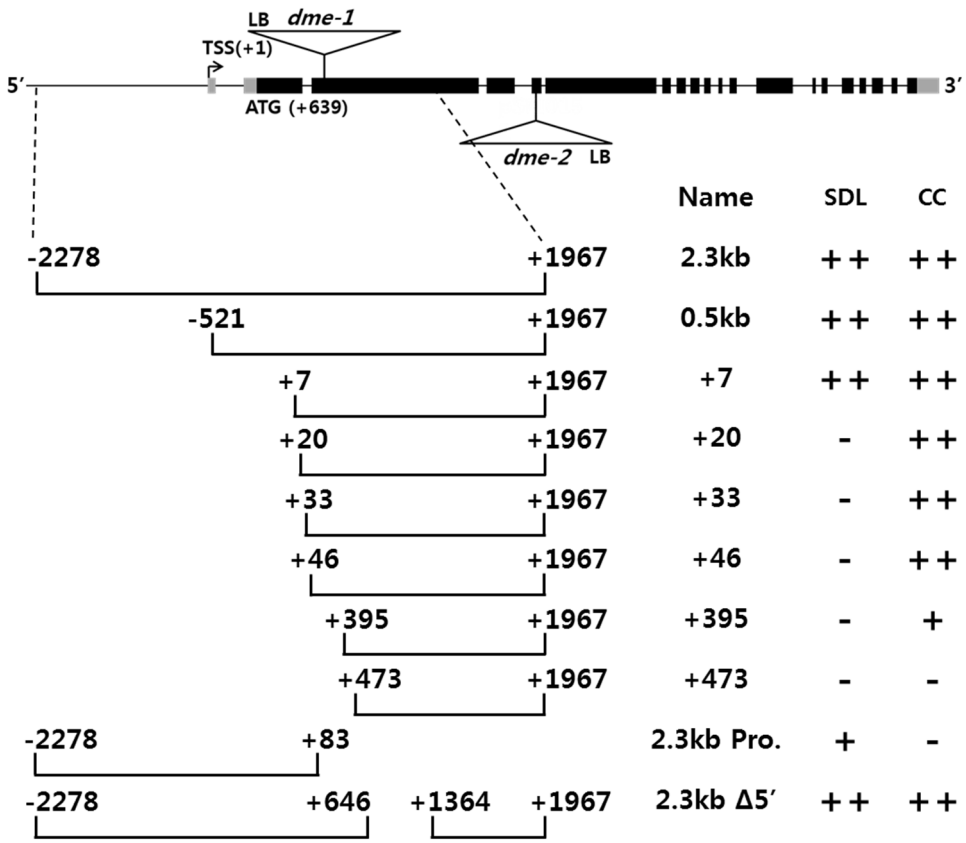

Figure 1-12. Diagram of the *DME::GUS* reporter construct series and their expression patterns.

SDL, seedlings; CC, central cells; [-, none; +, moderate; ++, strong]

Figure 1-13.

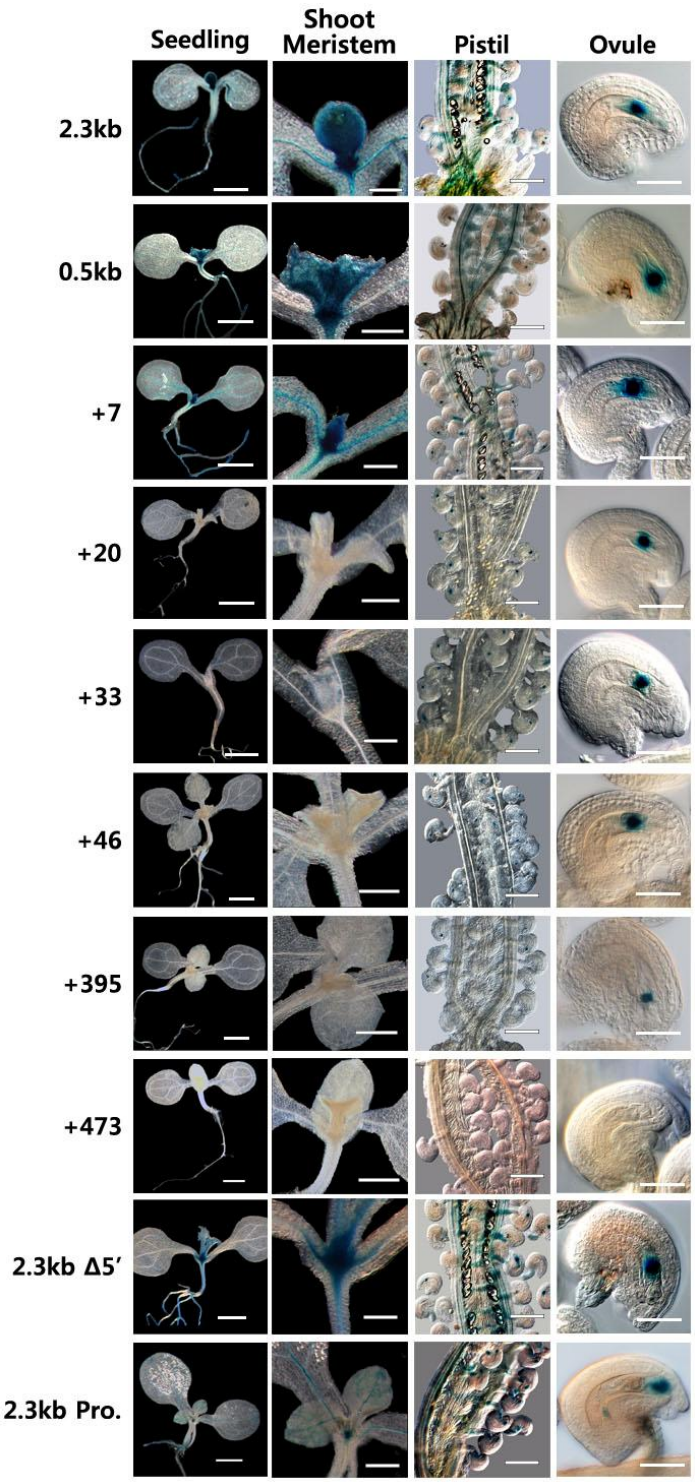
Seedling
Shoot Meristem
Pistil
Ovule
2.3kb
0.5kb
+7
+20
+33
+46
+395
+473
2.3kb Δ5′
2.3kb Pro.

Figure 1-13. Catalog of the Expression Patterns of the *DME::GUS* deletion series.

2.3 kb, *0.5 kb*, *+7 DME::GUS* and *2.3kb Δ5'* constructs showed *GUS* expression both in sporophytic tissues and central cells. +20, +33, +46 and +396 were expressed only in central cells. No expression was detected in +473 *DME::GUS* plants. 2.3 kb Pro. exhibited *DME:GUS* expression in sporophytic tissues, but not in the central cell nucleus. Ectopic expression was detected in the micropylar end of the embryo sac. Scale bars = 1000μm in (Seedling), 200μm in (Shoot meristem and Pistil), 50μm in (Ovule)

Figure 2-14

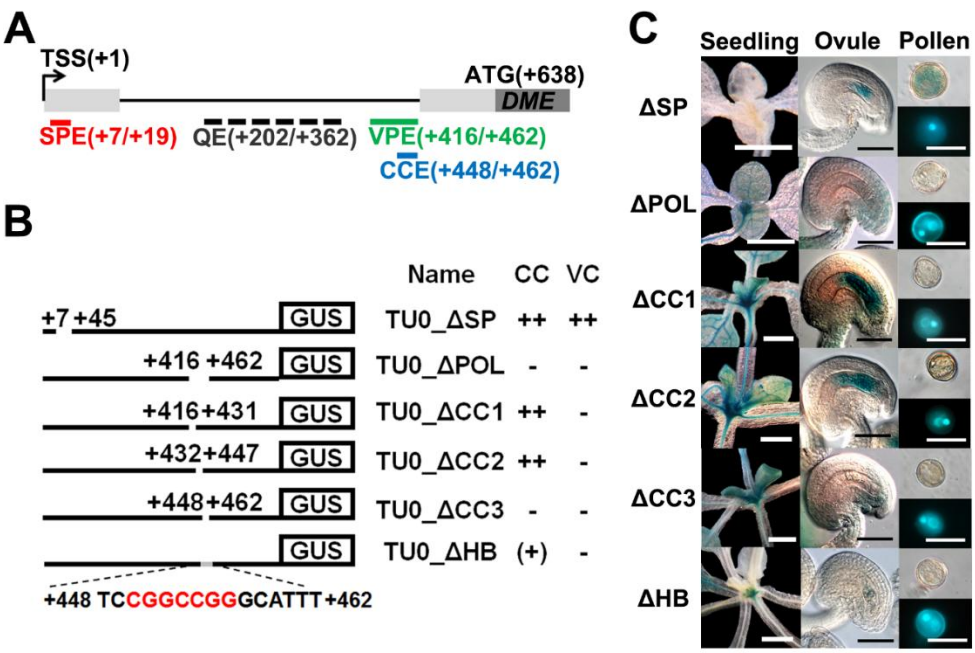

Figure 1-14. Internal deletion/substitution of the cis-elements.

(*A*) Summary of *DME* cis-regulatory elements. Dark gray box, translated exon; light gray box, 5'-UTR; first line, 5' flanking region; second line, 1st intron; red line, sporophytic element (SPE); blue line, central cell element (CCE); green, pollen vegetative cell element (VCE) ; dotted line; quantitative regulatory element (QE). (*B*) Diagram of *DME::GUS* internal deletion and substitution constructs of the cis-elements. CC, central cells; VC, vegetative cell of pollen; [-, none; (+), weak; ++, strong]; Δ, deletions or substitutions. (*C*) GUS staining is shown in ovules and pollen. DAPI-

stained pollen grains are shown in the bottom of each pollen. TU0_ΔSP, same GUS expression pattern as TU0; TU0_ΔPOL, central cell and pollen GUS disappeared; TU0_ΔCC1 and TU0_ΔCC2, only the pollen expression disappeared; TU0_ΔCC3, central cell and pollen GUS disappeared. TU0_ΔHB, central cell GUS was significantly reduced and pollen GUS disappeared. Scale bars = 1000μm in seedling, 50μm in ovule, 20μm in pollen.

1.3.6. Sequence Substitution Inside the SPE Region Abolishes Sporophytic Expression, and Binds the BPC3 Transcription Factor.

The *DME* SPE, (+7/+19), contains CT-repeats that are known targets of the BASIC PENTACYSTEIN (BPC) transcription factor family (Kooiker et al. 2005; Simonini et al. 2012; Monfared et al. 2011). BPC proteins also bind to CA repeats, but not to AT-repeats, to activate genes *in vivo* (Kooiker et al. 2005; Simonini et al. 2012; Berger et al. 2011). To investigate the possibility of BPC regulation in the CT-repeats of the *DME* SPE, I generated *TU0_ΔCA* and *TU0_ΔAT* plants in which the CT-repeats of the *TU0* construct were changed to CA- and AT-repeats, respectively (Figure 1-15*A*). The substitution from CT- to CA-repeats did not affect transgene expression, as indicated by GUS staining (Figure 1-15*B*). However, the conversion of CT- to AT-repeats abolished transgene expression in sporophytic tissues, but not in reproductive tissues (Figure 1-15*B*). Thus, the CT-repeats of the +7/+19 sequence are important for sporophytic *DME* expression, possibly through the recruitment of proteins

such as BPC.

To test the interaction between BPC proteins and *DME* promoter, I utilized the Yeast-1-Hybrid system to screen the seven BPC protein candidates against the 12 bp SPE sequence (Figure 1-16*A*). BPC3 was the only protein that bound to the SPE, and no BPC proteins bound to the VCE or CCE, demonstrating that distinct regulatory networks exist to control DME expression in the reproductive and sporophytic regions of the plant. These results suggest that BPC3 is likely to regulate the sporophytic expression of DME via a 12 bp regulatory element near to the TSS (Figure 1-16*B*).

Figure 1-15.

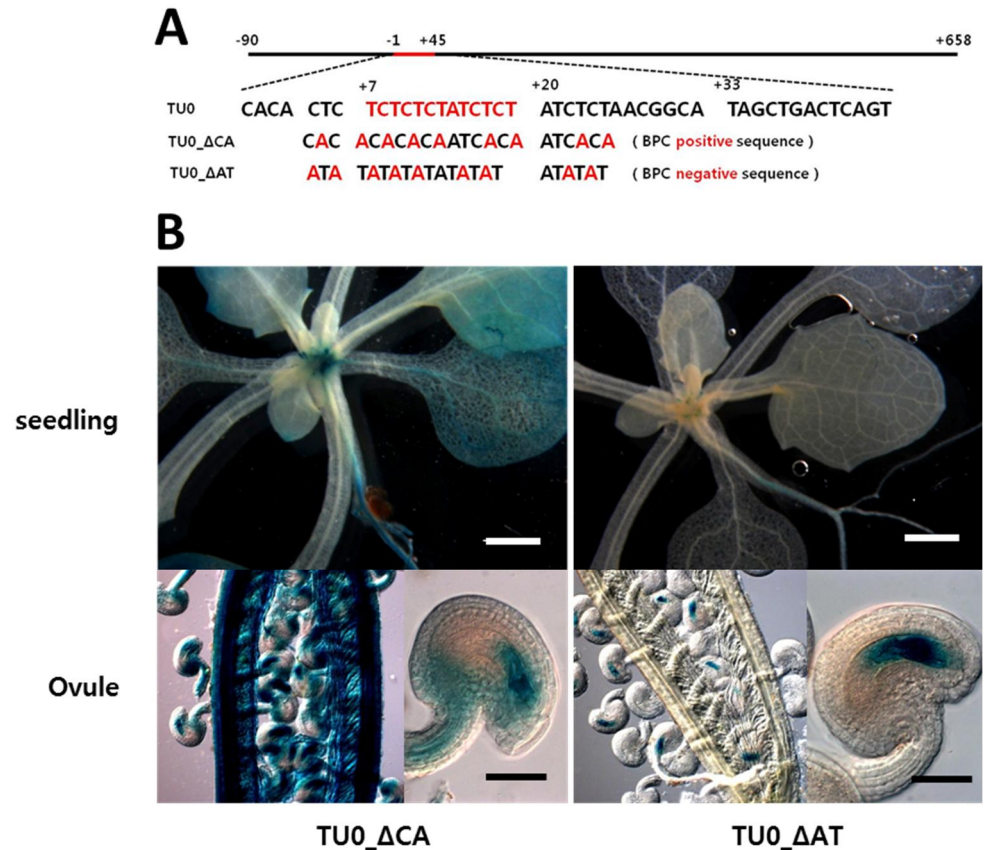

Figure 1-15. Expression analyses of the mutagenized cis-elements.

(*A*) Diagram of *DME::GUS* substitution constructs of the cis-elements. (*B*) GUS staining is shown in seedlings and ovules. TU0_ΔCA, same GUS expression pattern as TU0; TU0_ΔAT, seedling GUS disappeared. Scale bars = 1000μm in seedling, 50μm in ovule.

Figure 1-16.

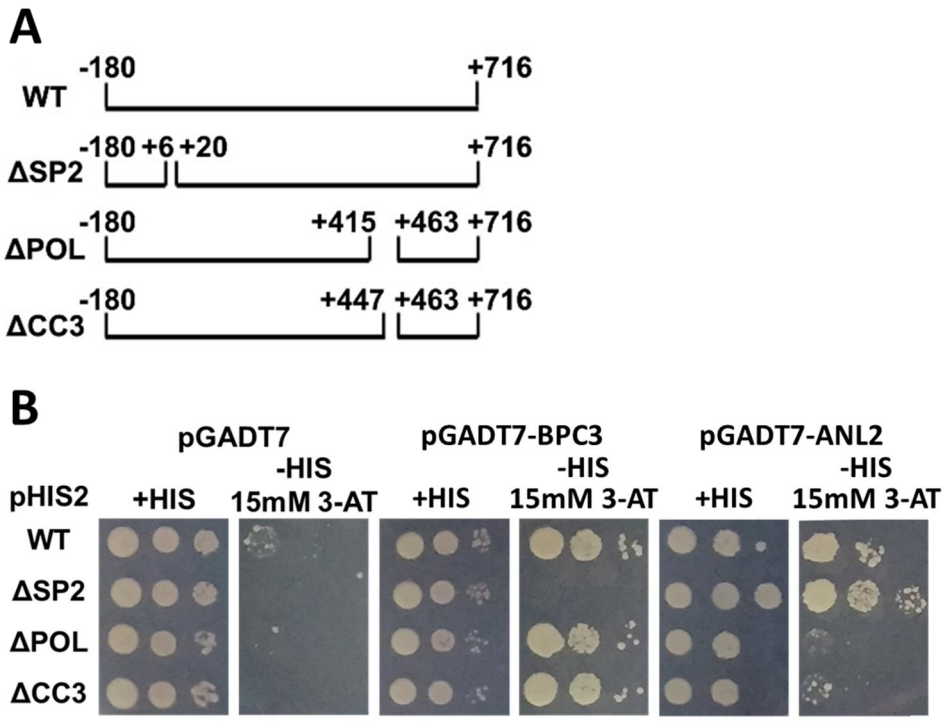

Figure 1-16. Internal deletion of the cis-elements and Yeast 1 hybrid assay with ANL2 protein.

(*A*) Diagram of constructs used yeast 1 hybrid assay. Each constructs were designed based on reporter expression. (*B*) Yeast 1 hybrid assay with BPC3 and ANL2 protein. BPC3 protein binds to pHIS2-WT, pHIS2-ΔPOL and pHIS2- ΔCC3, but not with pHIS2- ΔSP2. ANL2 protein binds to pHIS2-WT and pHIS2- ΔSP2 constructs, but not with pHIS2- ΔPOL and pHIS2- ΔCC3.

Figure 1-17.

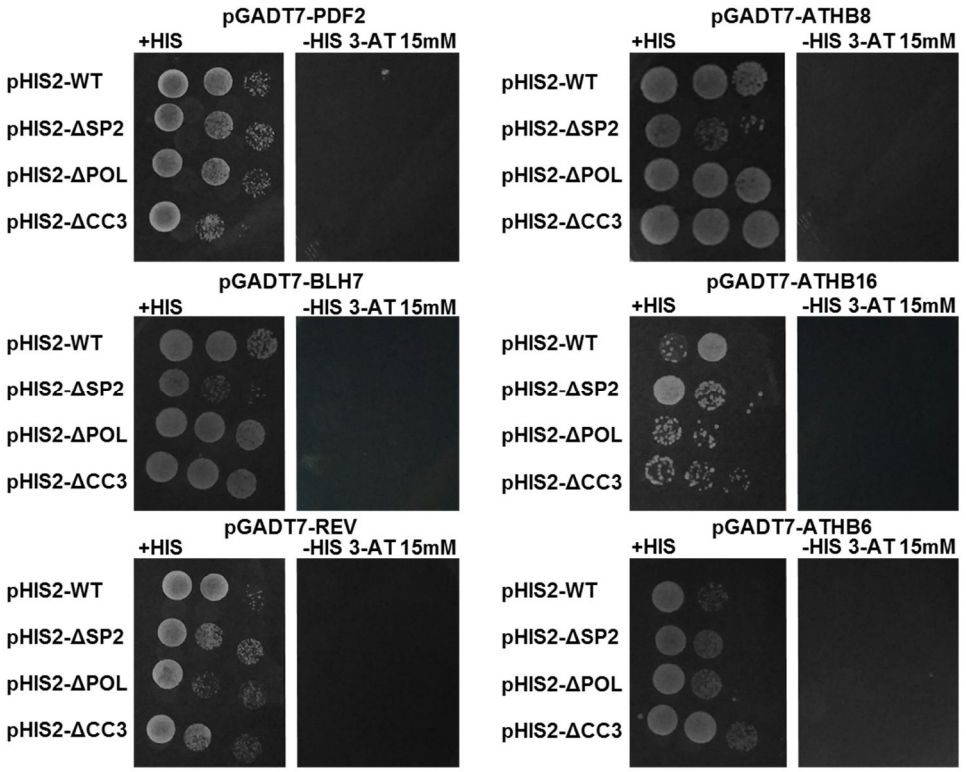

Figure 1-17. Yeast 1 hybrid assay with Homeobox (Sticker et al.) proteins.

Six HB protein candidates did not bind to pHIS2-WT, pHIS2- ΔSP2,

pHIS2- ΔPOL and pHIS2- ΔCC3 constructs.

1.3.7. Overlapping 15 and 47 Base Pair Regions Are Necessary for DME Expression in the Central and Vegetative Cells, Respectively.

As stated previously, a 57 bp element necessary for central cell DME expression lies between the +416 and +472 positions. To establish whether this sequence was also sufficient to drive *DME* expression, I generated constructs containing 1-4 copies of this 57 bp fragment with and without the minimal *CaMV* 35S promoter downstream, but none of these exhibited any GUS expression in any tissue, therefore I are unable to conclude that this sequence is sufficient for expression (Figure 1-18). Nevertheless, to investigate this region further, I generated fine-deletion constructs *TU0_ΔPOL* (Δ+416/+462), *TU0_ΔCC1* (Δ+416/+431), *TU0_ΔCC2* (Δ+432/+447) and *TU0_ΔCC3* (Δ+448/+462) (Figure 1-14*B*) to establish the sequence necessary for regulating central cell expression. GUS activity was detected in the central cell in *TU0_ ΔCC1* and *TU0_ΔCC2,* but not in *TU0_ΔCC3* or *TU0_ΔPOL* plants (Figure 1-14*B* and *C*), therefore the sequence necessary for central cell expression, denoted the CCE, is

approximately 15 bp in length and is located between +448 and +462 nt (Figure 1-14*A*). Vegetative cell *DME* expression is present in *TU0_ΔSP,* but disappears in *TU0_ΔPOL* and in each of *TU0_ΔCC1, TU0_ΔCC2,* and *TU0_ΔCC3* (VC in Figure 1-14*B* and *C*), demonstrating that vegetative cell expression of *DME* specifically requires the 47 bp +416/+462 sequence, denoted the VCE, which encompasses, but is broader than, the +448 /+462 CCE (Figure 1-14*A*).

Figure 1-18.

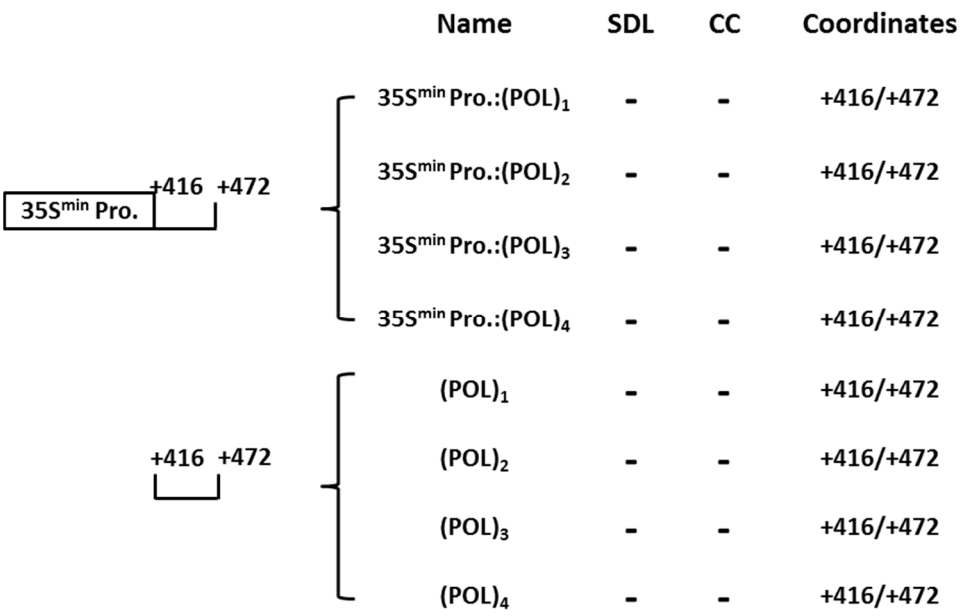

Figure 1-18. Diagram of the gain-of-function VCE tandem repeat constructs with and without the 35S minimal promoter.

A scheme is shown at left. The name of the construct is shown and the presence of staining in seedlings (SDL) and central cells (CC) indicated.

1.3.8. The 15 bp CCE Sequence, Shared by the VCE, Is Required for DME Expression and Is Predicted to Bind Several Key Transcription Factors.

DME expression in the vegetative and central cells is thought to have a common function, in regulation of transposon silencing in the germline. As such, the 15 bp common region of the VCE and CCE elements is of particular intrigue. This sequence contains the 9 bp 'CATTTATTG' motif, which is strikingly similar to the pseudo-palindromic targets of the *Arabidopsis* Homeobox HD-ZIP family of plant specific transcription factors; for example, the recognition sequence 'CAAT(T/A)ATTG' of subfamily 1 (Charite et al. 1998; Sessa, Morelli, and Ruberti 1993).

To examine the role of this AT-rich sequence in the expression of *DME*, 7 bp of AT-rich sequence in *TU0* was changed to GC-rich sequence (Figure 1-15). This change resulted in a significant reduction of GUS activity in the central cell of *TU0_ΔHB* plants and the complete absence of GUS expression in the vegetative cell of pollen (Figure 2-14*C*). Thus, the

pseudo-palindomic sequence is required for normal central and vegetative cell *DME* expression.

My identification of precise coordinates for key regulatory elements of DME expression enabled me to carry out preliminary investigations to reveal potential interacting transcription factors. A recent genome-wide analysis to characterize regulatory elements and transcription factor binding sites used a novel high throughput DNA affinity purification sequencing assay (DAP-seq), generating a 'cistrome' map for 30 % of transcription factors in *Arabidopsis* (O'Malley et al. 2016). By correlating my VCE and CCE coordinates with this cistrome dataset, I were able to identify 40 potential candidates that bind these regions *in vitro*, and may therefore be involved in DME regulation in reproductive tissues (Table 1-5). Among these candidates are 10 HD-ZIP transcription factors, spanning the four subfamilies, which is consistent with my finding functional targets of the HD-ZIP family in the common region of the VCE and CCE elements.

Of the homeobox genes in the Arabidopsis genome, the HD-ZIP proteins are the largest group, containing 46 individual genes, arranged into four sub-families (Ariel et al. 2007). Examining members of all four subfamilies, I used previously published expression data (Wuest et al. 2010) to choose putative HD-ZIP transcription factors that might bind to the *DME* promoter based on their expression patterns. I identified seven candidates that were expressed similarly to DME in the female gametophyte. Then, using a Yeast-1-Hybrid assay and cloning expression constructs for each candidate, I screened their binding ability to the 15 bp CCE. ATHB6, ATHB8, ATHB16, REV, PDF2 and BLH7 (a BELL family member) did not bind (Figure 1-17). However, ANL2 was found to bind to the CCE sequence within the VCE enhancer, but not to the CCE-deleted control sequences, allowing me to highlight ANL2 as one of the prospective transcriptional regulators of *DME* expression (Figure 1-16). I examined the siliques of several independently derived and confirmed homozygous *anl2* mutant T-DNA insertion lines, and did not observe any

seed abortion, therefore it seems likely that ANL2 acts redundantly in this pathway.

Table 1-5. Trans-element candidates of CCE/VCE binding from published DAP-seq data

Name	AGI	DAP-seq[1]	VCE reads [2]
HD-ZIP I			
ATHB23	AT1G26960	**	11F6R
ATHB6	AT2G22430	*	2F4R
ATHB40	AT4G36740	*	2F2R
LMI1	AT5G03790	*	9F18R
HD-ZIP II			
HAT22	AT4G37790	*	4F1R
HD-ZIP III			
ATHB15	AT1G52150	*	5F
PHB	AT2G34710	*	5F1R
ATHB8	AT4G32880	*	5F 8R
HD-ZIP IV			
ANL2	AT4G00730	**	10F10R
HDG4	AT4G17710	*	3F5R
KNOX			
KNAT1	AT4G08150	*	5F8R
WOX			
WOX4	AT1G46480	*	1F1R
bHLH			
HEC3	AT5G09750	*	6R
bZIP			
TGA3	AT1G22070	*	4R
CAMTA			
CAMTA2	AT5G64220	*	3F6R
DBP			

DBP	AT3G51470	*	1F3R
FAR1			
FAR1_FRS12	AT5G18960	*	5F
FHA			
FHA	AT2G21530	*	5R
FHA	AT5G47790	*	4R
GEPB			
GEPB	AT4G25210	*	5F6R
GRF			
GRF6	AT2G06200	*	5F9R
HSF			
HSFA6A	AT5G43840	*	1F4R
HSFA4C	AT5G45710	*	1F2R
MADS			
AGL63	AT1G31140	***	19F20R
AGL11	AT4G09960	*	2F6R
AGL98	AT5G39810	*	5R
AGL52	AT4G11250	*	23F15R
AGL23	AT1G65360	*	5R
MYB-LIKE			
HD-like	AT4G01280	***	15F12R
EPR1	AT1G18330	***	26F27R
LCL1	AT5G02840	***	26F24R
LHY1	AT1G01060	***	14F15R
RVE1	AT5G17300	***	14F13R
LCL5	AT3G09600	***	27F28R
HD-like	AT3G10113	***	19F27R
NAC			

ANAC018	AT1G52880		8F9R
ORPHAN			
ARR22	AT3G04280	***	9F12R
REM			
REM19	AT1G49480	*	16F13R
REMB3	AT2G31460	*	5R
SBP			
SLP1	AT1G07010	*	7F

[1]Factors were included if the center of the VCE element overlapped with the peak of the reads. Peak size is indicated by number of *, with * indicating a minor peak and * indicating distinctive peak.**

[2] Reads are then listed here as the number on the forward strand (F) and the number on the reverse strand (R). Reads were normalized according to (O'Malley et al. 2016).

1.4. Discussion

Here, I show that the regulation of DME expression is mirrored in both male and female gametophytes, developing simultaneously upon germline differentiation in distinct reproductive organs. *DME* expression is restricted to the vegetative cell nucleus after the first asymmetric mitosis, at the late bi-cellular stage of pollen development (Figure 1-1). This is concurrent with separation of the generative and vegetative cell lineages, so that the demethylation activity of DME is restricted to the vegetative cell, while the sperm genome remains highly methylated at DME targets. This expression profile is likewise reflected in the female gametophyte. During female gametogenesis, the third mitotic division is followed immediately by cellularization and differentiation, generating antipodal cells at the chalazal pole, and the egg cell, synergids and two polar nuclei at the micropylar pole (Drews and Koltunow 2011). It is immediately after this differentiation step that *DME* expression is activated, so that

expression is confined primarily to the polar nuclei, which fuse to form the central cell, and is absent from the egg (Choi et al. 2002a).

Expression of *DME* in companion cells, and the evasion of *DME* expression in gametes, is key for understanding the function of DNA demethylation during plant reproduction. This pattern explains how the maternal endosperm genome is hypomethylated compared to the paternal endosperm genome. Maternally hypomethylated loci are either directly or indirectly (via PRC2 activity) responsible for parent-of-origin gene expression, i.e. gene imprinting, in the endosperm (Hsieh et al. 2009; Hsieh et al. 2011). The fact that *DME* is not expressed in the egg or sperm cells is responsible, at least in part, for the similarity of the maternal and paternal embryo methylomes (Ibarra et al. 2012) and, therefore, the fact that genes displaying parent-of-origin expression in endosperm do not do so in the embryo (Hsieh et al. 2011; Gehring, Missirian, and Henikoff 2011). Maternal genome hypomethylation is required for seed development, but the demethylation of the vegetative cell does not directly

affect seed viability. Instead, demethylation of both the central and vegetative cells at DME targets; small, AT-rich, and nucleosome-depleted euchromatic TEs, likely promotes expression of TEs in these cells. Demethylated companion cells do not pass on their genome to the next generation; therefore, the genomic instability resulting from transposon transcription is not deleterious to the species as a whole. Rather, there is evidence to suggest that the RdDM pathway then promotes corresponding TE methylation in the egg and sperm cells respectively (Ibarra et al. 2012; Slotkin et al. 2009; Martínez et al. 2016). In this way, the companion cell acts sacrificially, reinforcing and protecting the genomic integrity of egg and sperm, which will be inherited by the next generation. The function of *DME* expression in companion cells provides support for the unique importance of double fertilization involving companion cells during evolution.

I explored the regulatory sequences that contribute to this

remarkable expression profile by producing a comprehensive array of iteratively deleted reporter transgenes for the regions upstream of the *DME* translational start site. With the exception of a negative regulatory region that suppresses *DME* expression in female gametophyte synergid cells, all other regulatory elements reduced *DME* expression when lost or mutated (Figure 1-3 and 1-8), suggesting that the majority of transcriptional regulation of *DME* is positive. The lack of DME expression in the fertilized endosperm, needed to preserve regions of DNA demethylation that are specific to the maternal endosperm genome (Ibarra et al. 2012), is therefore likely caused by a decrease in activity of a positive regulator or regulators, rather than the appearance of a negative regulator.

Using my deletion transgenes, I found that sequences regulating *DME* expression were contained within its transcriptional unit. I designated the +46 transgene; which consists of 592 bp of sequence before the translational start site, as the minimal reproductive promoter and

utilized this in a functional construct to drive expression of *DME* cDNA. The expression of this transgene rescued both the seed abortion and genome-wide DNA methylation phenotypes of *dme-2* heterozygous and homozygous mutants, showing that the expression timing, level and tissue specificity of *DME* expression in reproductive tissues is recapitulated with a promoter sequence of 592 bp contained within the transcriptional unit. Within this sequence I identified a 47 bp VCE, overlapping with a 15 bp CCE, necessary for regulation of the vegetative and central cell DME expression patterns, respectively. The CCE and VCE are distinct from the 13 bp SPE close to the TSS that promotes DME expression in the sporophyte. Each of the three enhancer sequences are conserved in closely related *Brassicaea* family members, such as *Arabidopsis lyrata*, *Capsella rubella* and *Brassica rapa* (Figure 1-19), but they are missing from the *DME* homologues *ROS1, DML2,* and *DML3*, which are expressed much more broadly than *DME* (Penterman et al. 2007) and do not contribute to demethylation in the central cell.

Figure 1-19

Figure 1-19. DME and *ROS1* homolog comparisons in publically available Brassica family DNA sequences.

Lines above the DNA sequence indicate the cis-regulatory elements found by these experiments. SPE in the *DME* CT-repeats (red box) and the 9 bp of sequence that is similar to the pseudo-palindromic target sequence that is similar to Arabidopsis thaliana Homeobox 1(Athb-1) (blue box) are well conserved in Brassica family. A.Th, *Arabidopsis thaliana*; A. Ly, *Arabidopsis lyrata*; C.Ru, *Capsella rubella*; B.Ra, *Brassica rapa*.

As the CCE is contained entirely within the VCE, it is possible that the control of *DME* expression in each of the companion cells of the gametes shares a common regulatory pathway. The overlapping VCE/CCE sequence of 15-bp (+448/ +462) is AT rich, including 9 bp with striking similarity to the pseudo-palindromic 'CAAT(T/A)ATTG' sequence, which is a target of the HD-ZIP plant specific homeobox transcription factor family (Chan et al. 1998; Palena, Gonzalez, and Chan 1999; Palena et al. 2001). Substitution of this motif led to a large reduction in central cell *DME* expression and ablation of vegetative cell *DME* expression, showing that this pseudo-palindromic sequence is required for correct DME regulation.

Using the coordinates that I derived for the VCE and CCE and my analyses of the recently published DAP-seq 'cistrome' collection (Hehenberger, Kradolfer, and Kohler 2012) I was able to catalogue a list of 40 potential transcription factors, including 10 HD-ZIPs, that bind to these elements *in vitro* (O'Malley et al. 2016). MADS-box transcription factor

AGL80 is required for *DME* expression in the central cell (Portereiko et al. 2006), so it is likely that MADS-box binding domains are present in this regulatory region, and several MADS-box transcription factors were found to bind to the VCE by DAP-seq (Table 1-5) (O'Malley et al. 2016), however AGL80 was not specifically tested in the DAP-seq screen.

If there is a transcription factor that co-regulates *DME* in the central and vegetative cells, it would be expressed in both these tissues, at a similar time to DME itself. However, as I show here, DME expression in the male gametophyte is confined to a short period of the bicellular pollen stage and is often not detected in pollen expression datasets (Borges et al. 2008; Qin et al. 2009; Boavida et al. 2011). Thus, to identify potential transcription factors that may bind the shared sequence of the VCE and CCE and regulate DME, precise establishment of their endogenous expression profile using reporter genes will be required in the future.

In summary, I show here that *DME* expression during reproduction is confined to a narrow window of time, and to single companion cells, in

female and male gametophytes, which is necessary for its role in seed viability, gene imprinting, and transgenerational transposon silencing. I delineate specific, conserved enhancer sequences required for the precise expression pattern of *DME*, and identify candidate transcription factors by their *in vitro* binding patterns at the VCE and CCE, information that will be valuable in the future to delineate the regulatory pathways that control DME expression.

II. Chapter II.

Interaction between DNA demethylase family members in *Arabidopsis thaliana*

2.1 Introduction

DNA methylation is an evolutionarily conserved epigenetic mechanism that controls numerous biological processes. The methylation level is dynamically controlled by establishment, maintenance and demethylation. In plant, these three processes are well understood. The establishment of DNA methylation is mediate through RNA-directed DNA methylation (RdDM) pathway. According to the current understanding of canonical RdDM in *Arabidopsis thaiana* the production of 24-nucleotide siRNAs is initiated through transcription by RNA POLYMERASE IV (POL IV). Then, RNA- DEPENDENT RNA POLYMERASE 2 (RDR2) copy of the transcript to generate a double stranded RNA (dsRNA). And cleavage of the dsRNA into siRNAs by DICER- LIKE PROTEIN 3 (DCL3) (Law and Jacobsen 2010) (Matzke and Mosher 2014) (Zhang and Zhu 2011) (Pikaard et al. 2012).

Maintenance of DNA methylation use different pathway depends on sequence context. Methyltransferase 1 (MET1) do maintenance of CG

methylation. MET1 recognizes hemi- methylated CG dinucleotides following DNA replication and methylates the unmodified cytosine in the daughter strand (He, Chen, and Zhu 2011). CHG Methylation is maintained by the DNA methyltransferase CHROMOMETHYLASE 3 (CMT3) (Woo, Dittmer, and Richards 2008). CHH methylation is maintained by DOMAINS REARRANGED METHYLASE 2 (DRM2) or CMT2. DRM2 maintain the methylation of RdDM target. And CMT2 target a methylation at histone H1-containing heterochromatin, where RdDM is inhibited (Jeddeloh, Stokes, and Richards 1999).

DNA demethylation occurs either by passive or active process. Passive DNA demethylation occurs during DNA replication without DNA methylation maintenance. Passive DNA demethylation has been reported during gametophyte development (Zhu 2009). Active DNA demethylation involves the enzymatic removal of methylated cytosine. In plants, this process is initiated by a family of DNA glycosylases including Demeter (DME), Repressor of silencing 1 (ROS1), Demeter-like 2 (DML2), and

Demeter-like 3 (DML3). A base excision repair (BER)-dependent mechanism then completes the process(Penterman et al. 2007; Zhu 2009).

DME, ROS1, DML2, and DML3 are bi-functional DNA glycosylases involved in BER. *ROS1*, *DML2*, and *DML3* are ubiquitously expressed in vegetative tissues and exhibit partial functional redundancy (Zhu et al. 2007; Penterman et al. 2007; Ortega-Galisteo et al. 2008). As my study, DME is also expressed in vegetative tissues. An Arabidopsis triple mutant of *ROS1*, *DML2*, and *DML3* (*rdd*) showed DNA hyper-methylation (increased level of methylated cytosine) at nearly 9000 loci, which was a considerably higher number than the number of loci specifically targeted by ROS1 (approximately 5000) (Qian et al. 2012), suggesting that DML2 and DML3 also have unique functions. So, I thought that DME may have a functional redundancy in vegetative tissues. And I want to know about interaction of four DNA demethylases. To identify interaction between DME homologues, I crossed these mutants each other. Our data indicate that ros1-3, dml2-1 and dml3-1.

2.2 Materials and methods

2.2.1. Plant materials and growth conditions

The *dme-1* homozygous mutant allele is in Landsberg *erecta* (L*er*) background (Choi et al. 2002a). Heterozygous *dme-2* in L*er* and Col-*gl* was used for the cross. Triple homozygote *ros1-3*; *dml2-1*; *dml3-1* is Columbia-*glabrous* (Col-*gl*) background (Penterman et al. 2007). The plants were grown in either long-day (16hour light / 8hour dark) or short-day (8hour light / 16hour dark) photoperiodic conditions under cool white fluorescent light (100 μmole/m^2/s) at 22°C with 60% relative humidity.

2.2.2. Gene expression analysis

Total RNAs were isolated using RNA queous^{TM} (Ambion). After RNase-free DNase (TaKaRa Bio) treatment, 4ug total RNAs were used to synthesize cDNA using oligo-dT primers and M-MLV reverse transcriptase (Ambion). RNA levels were quantified by PCR. For control normalizations, I used *UBIQUITIN10* (*UBQ10*) gene expression (Table 1-

1).

2.3 Results

2.3.1 Strong allele *dme-2* homozygous mutants are able to be generate by cross with weak allele dme-1 mutants.

The *dme-2* allele is a stronger allele than *dme-1* because of its T-DNA location (Figure 2-1). The T-DNA insertion in *dme-1* is in the 5'- exon at the boundary of the 5'-untranslated region in *DME.1* model (Figure 3-1) (Choi et al. 2002a). Thus, it is possible that transcription and translation starting from sequences in the T-DNA of the *dme-1* allele might result in low level production of active, near full-length DME protein. By contrast, the T-DNA insertion in *dme-2* is in an exon in the middle of the *DME* gene (Figure 2-1), suggesting that no functional DME protein can be made. For this reason, *dme-1* homozygous mutant was made although in a rare chance. However, *dme-2* homozygous mutant was not found in a natural condition. In order to study the function of DME in sporophytic tissues, the stronger homozygous *dme-2* mutant might be more useful than weaker *dme-1* allele.

Figure 2-1.

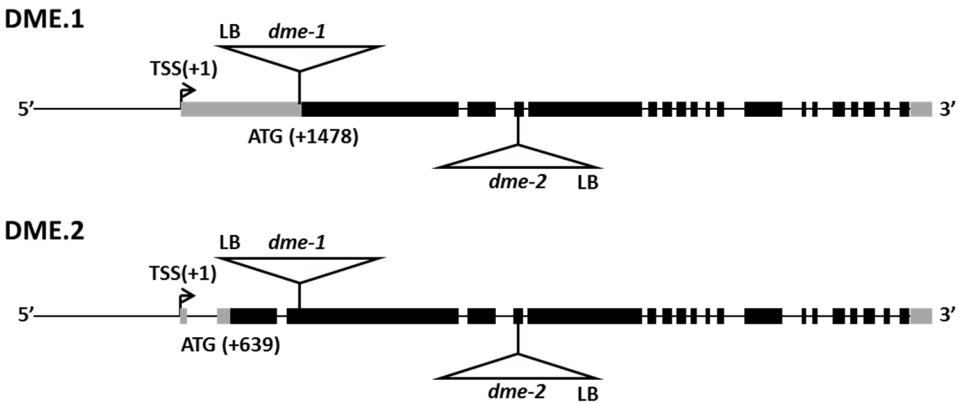

Figure 2-1. Diagram of *dme* mutant allele.

The number is based on the transcription start site of each gene model. Gray box, 5' and 3' UTR; black box, translated exon; front line, 5'flanking region; line between boxes, intron; triangle, T-DNA inserted into *DME* gene; TSS, transcription start site; LB, left border of T-DNA.

My strategy to obtain the *dme-2* homozygous mutant was based on the allele competition between *dme-1* and *dme-2*. In a self-cross situation of the *dme-2* heterozygous plant, *dme-2* allele competes with wild type DME gene. But in case of *dme-1* and *dme-2* hybrid mutant, the *dme-2* allele would compete with the *dme-1* allele which also has a defect. Thus, this strategy would increase the probability of creating *dme-2* homozygous mutant.

I used dme alleles in Landsberg *erecta* (L*er*) background because there is no male defect observed in L*er* background. Only the maternal seed abortion is observed when mutant allele is transmitted through female in L*er*. By contrast, dme allele in Columbia-*glabrous* (Col-*gl*) background also showed defect in pollen germination (Schoft et al. 2011). Therefore, it would be easier to get *dme-2* homozygous mutant in L*er* than that in Col-*gl* background. Consistent with this, *dme-1* homozygous mutant was also discovered in L*er* background. When the first *dme-1* homozygous mutant

was discovered, it showed over 95% seed abortion ratio. Interestingly, this low seed viability did increase through generations. The *dme-1* plants used in this experiment had been in a homozygous state approximately more than 15 generations. They showed drastic lower seed abortion ratio which was about 56 %. Meanwhile, *dme-2* heterozygous plant did show approximately 50% seed abortion and no maternal mutant allele transmission occurred (Table 2-1).

Homozygous *dme-1* plants were used as female parents and *dme-2* heterozygous plants were used as male parents. As a result, we could get three viable seeds and these were planted and genotyped the plants. Among three plants, only one was confirmed to be *dme-1*/*dme-2* hybrid mutant. Other two plants were *dme-1*/+. The seed abortion ratio of this *dme-1*/*dme-2* hybrid plant was around 76%. This abortion ratio seems to be the average value of the first discovered homozygous *dme-1* plant (> 95 %) and the most recent *dme-1* homozygous plant (~ 56 %) that showed alleviated seed abortion phenotype when the multiple generation went

through.(Table 2-1)

Table 2-1. Seed abortion in *dme* alleles.

Genotype	Total viable seed	Total aborted seed	Average seed abortion ratio (%) ± SD
dme-1/dme-1	118	150	56.0 ± 9.5
dme-2/DME	152	123	44.7 ± 3.7
dme-1/DME (F1-1)	125	81	39.3 ± 9.1
dme-1/dme-2 (F1-3)	60	191	76.1 ± 10.5
dme-1/dme-1 (F2)	122	1306	91.5 ± 4.8
dme-1/dme-2 (F2)	46	1370	96.8± 3.1
dme-2/dme-2 (F2)	38	1284	97.1± 2.4

The hybrid plant was self-pollinated and the segregating F2 generations were all genotyped to examine the transmission of each allele and to find homozygous *dme-2* plant. The F2 progeny of the *dme-1*/*dme-2* hybrid mutants showed 25 (39.7 %), 31 (49.2 %), and 7 (11.1 %) of *dme-1* homozygote, *dme-1*/*dme-2* hybrid, and *dme-2* homozygote, respectively. This result also confirmed that the transmission of *dme-2* allele was significantly lower than that of *dme-1* allele. The F2 progeny of the *dme-1* heterozygote obtained in this cross showed 63 (54.8 %), 51 (44.3 %) and 1 (0.9 %) for wild type, *dme-1* heterozygote, and *dme-1* homozygote, respectively (Table 2-2).

Seed abortion ratio of the F2 generation was different from that of F1. The average abortion ratio of F2 *dme-1* homozygote was 91.5% whereas *dme-1* / *dme-2* hybrid showed 96.8% and *dme-2* homozygous mutants displayed 97.1% (Table 2-1). In this generation, we could also get a new *dme-1* homozygous mutant that came from the heterozygous *dme-1* plant, which is a segregant of *dme-1* homozygote and *dme-2* heterozygote

cross. This newly obtained homozygous *dme-1* plants displayed approximately 90% seed abortion phenotype, indicating that the alleviated seed abortion observed in the later generation of the *dme-1* homozygous plants has disappeared (Table 2-1).

Table 2-2. Segregation of F2 population

		F1		
		DME/dme-1		***dme-1/dme-2***
	DME/DME	**63(54.8%)**	***dme-1/dme-1***	**25(39.7%)**
F2	***DME/dme-1***	**51(44.3%)**	***dme-1/dme-2***	**31(49.2%)**
	dme-1/dme-1	**1(0.9%)**	***dme-2/dme-2***	**7(11.1%)**

2.3.2. Backcrossing of L*er* dme-2 homozygous mutant with Col-gl dme-2 heterozygous mutant is not able to eliminate Ler genome.

Since the transmission of dme mutant allele through male is comparable to WT in L*er* background, but not in Col-*gl* background, that might be one of the reasons of obtaining *dme* homozygous mutant in L*er*, at least in part. To generate *dme-2* homozygous mutant in Col-*gl* background as well as to investigate why these two ecotypes show the difference in dme mutant allele transmission, an experiment was designed by using the *dme-2* L*er* homozygous plants to generate *dme-2* homozygous mutant in Col-*gl*. The strategy was; *dme-2* homozygous plants in L*er* would be crossed with Col-*gl* *dme-2* heterozygous pollen to obtain an *dme-2*/*dme-2* ecotype hybrid (Figure 3-2). Then, this *dme-2*/*dme-2* ecotype hybrid plants would be crossed five times with pollen from Col-*gl* *dme-2* heterozygous plants. Eight out of 50 individuals from the first cross were *dme-2* homozygote (L*er*/Col-*gl*), which were then subjected to a second cross with Col-*gl* *dme-2* heterozygous plants. Since the second cross was not successful

(only 1 seed was obtained, but it was heterozygote.), the plants were let self-pollinated to produce more offspring. 30 plants of this BC1 F2 generation were obtained and backcrossed with Col-*gl* heterozygous *dme-2* again. They produced 80 seeds. Although the third cross was attempt, 8 viable seeds were obtained, but they were heterozygote as the second cross. This indicates again if the Col-*gl* genome is introduced, it is more difficult to get homozygous *dme-2* mutants in Col-*gl* background. Another self-cross generation was produced which I called BC2 F2. 11 seeds germinated from 4 parents and from these plants backcross with Col-*gl* heterozygous *dme-2* was substantially successful. Finally, 18 Col-*gl* based *dme-2* homozygous plants were produced (Figure 2-2).

Figure 2-2.

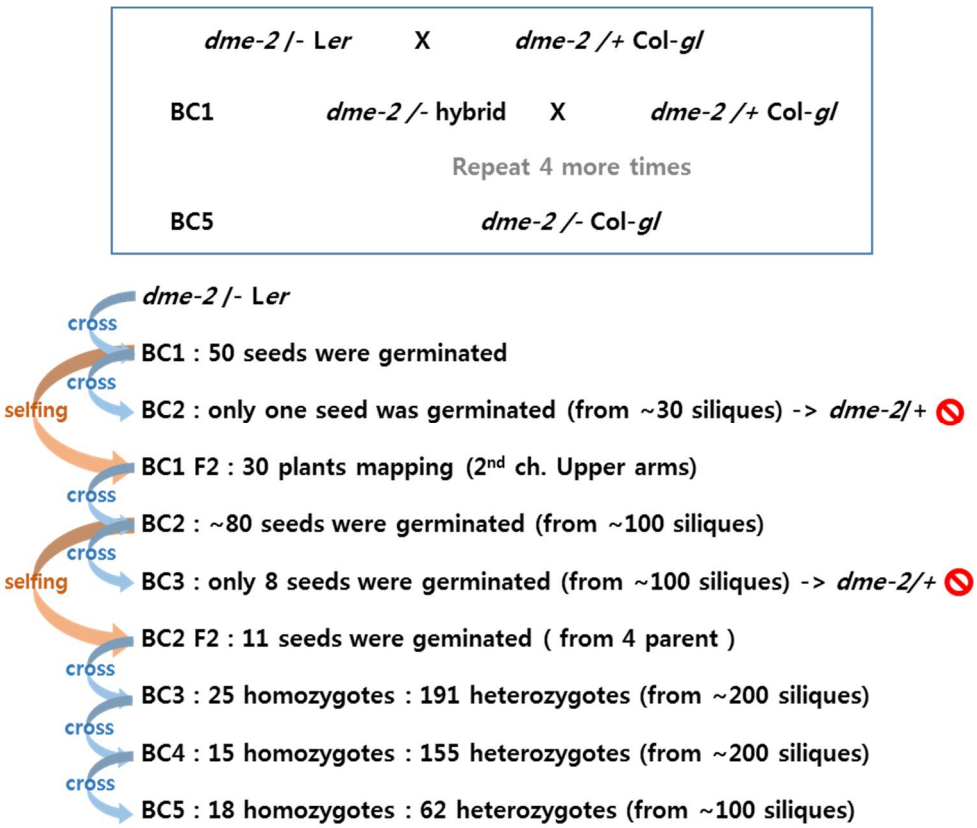

Figure 2-2. Backcross strategy and progress of L*er* dme-2 homozygous mutant and Col-*gl* dme-2 heterozygous mutant.

BC; backcross generation, blue arrow; backcross, orang arrow; self-pollinated, red circle; could not obtain dme-2 homozygous mutant.

Genetic mapping was performed to identify L*er* and Col-*gl* genome composition in *dme-2* homozygous mutants during these crosses. In addition, this would tell me the loci, if any, which increase seed viability in *dme-2* L*er* homozygous mutants. 30 plants from BC1 F2 were first mapped (Figure 2-3 and 2-4). The result showed that chromosome 2 had more L*er* genome than others. The marker nga162, located in the upper arm of chromosome 3, as well as ciw9 and ciw10 which are both in the lower arm of chromosome 5 displayed 10 % higher in L*er* than average. The markers for the upper arm of chromosome 5 were fully Col-*gl* because of the origin of the *dme-2* allele.

18 plants obtained after 5 backcrosses (BC5 F1) were also mapped to find any differences (Figure 2-5). Every L*er* element was compared with the mapping result of BC1 F2. The overall L*er* ratio of chromosome 2, which was high-L*er* in the former case, was significantly reduced. On the contrary, ciw12 and nga111, which was about 50% in BC1 F2, became L*er*-dominant. nga162, ciw9, and ciw10 markers that were relatively L*er*-

high in the previous mapping remained still high for L*er* genome. In order to analyze whether these high L*er* section helps *dme-2* seeds to survive, fine mapping between ciw9 and ciw10 was performed. As a result, the highest proportion of L*er* elements was found to be closer to ciw9 than to ciw10. There is *MET1* methyltransferase gene between ciw9 and ciw10, but the peak position slightly differed from the *MET1* gene region.

Figure 2-3.

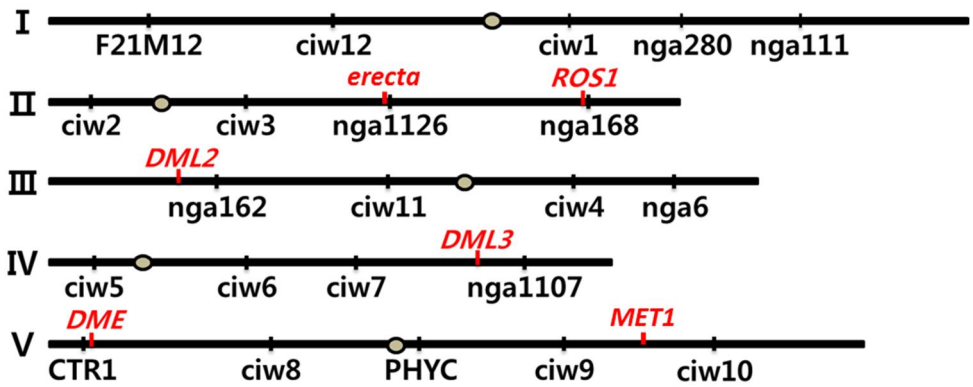

Figure 2-3. Diagram of marker used mapping and locus of some genes of interest.

Roman numerals mean chromosome number. Circles; on bar are centromere.

Figure 2-4.

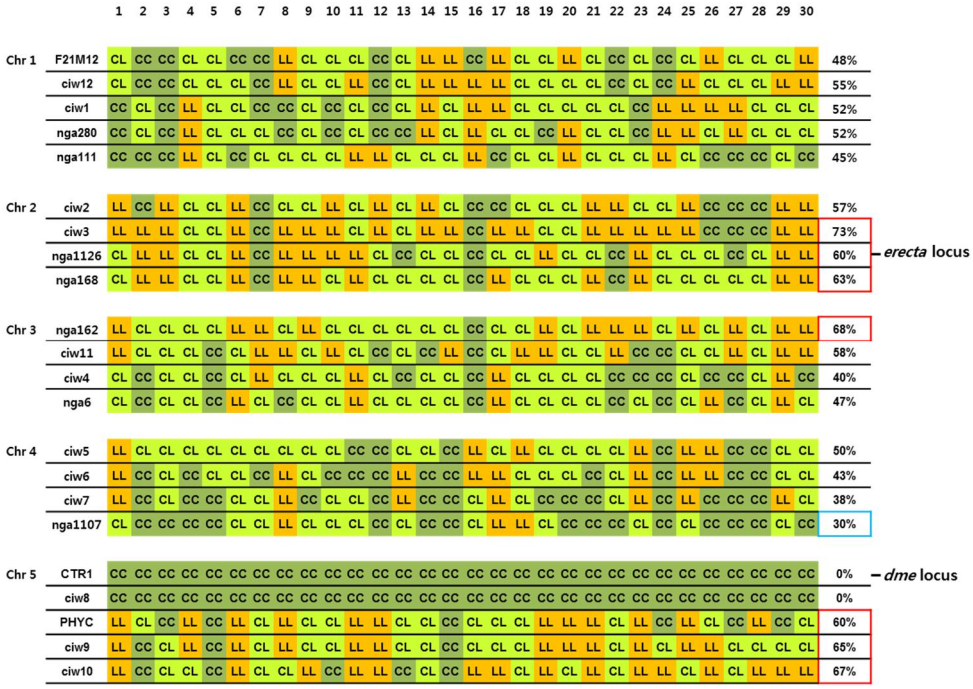

Figure 2-4. Result of BC1 F2 mapping.

30 plants, that were self-pollinated after one backcross of L*er* dme-2 homozygote and Col-*gl* dme-2 heterozygote, were mapped. List of markers is the leftmost column, and the number in rightmost column represents L*er* ratio for each marker locus. Red box; 10% higher in L*er* than average, blue box; lowest in L*er*, CC; Col/Col, CL; Col/L*er*, LL; L*er*/L*er.*

Figure 2-5.

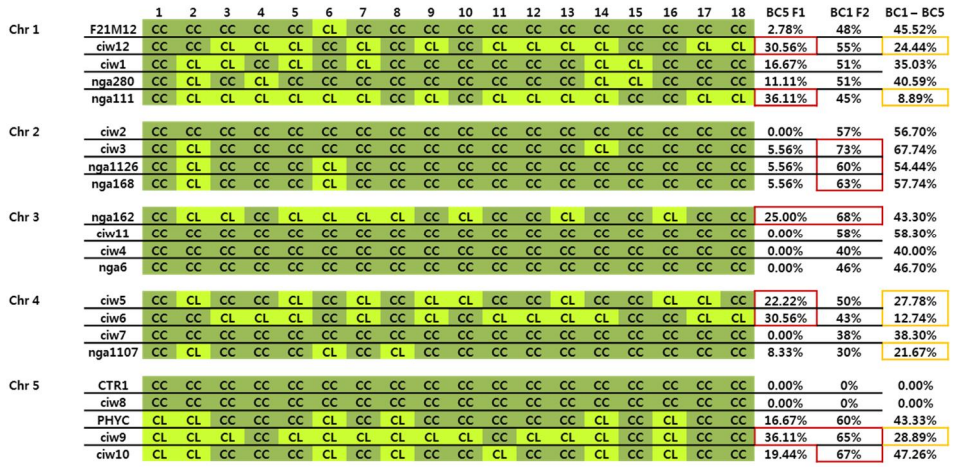

		1	2	3	4	5	6	7	8	9	10	11	12	13	14	15	16	17	18	BC5 F1	BC1 F2	BC1 – BC5
Chr 1	F21M12	CC	CC	CC	CC	CC	CL	CC	CC	CC	CC	CC	CC	CC	CC	CC	CC	CC	CC	2.78%	48%	45.52%
	ciw12	CC	CC	CL	CL	CL	CC	CL	CC	CL	CC	CL	CL	CL	CL	CC	CC	CL	CL	30.56%	55%	24.44%
	ciw1	CC	CL	CL	CC	CL	CC	CL	CC	CC	CC	CC	CC	CC	CL	CL	CC	CC	CC	16.67%	51%	35.03%
	nga280	CC	CL	CC	CL	CC	CC	CC	CC	CC	CC	CC	CC	CC	CL	CL	CC	CC	CC	11.11%	51%	40.59%
	nga111	CC	CL	CL	CL	CL	CL	CL	CC	CL	CC	CL	CL	CL	CL	CC	CC	CL	CL	36.11%	45%	8.89%
Chr 2	ciw2	CC	CC	CC	CC	CC	CC	CC	CC	CC	CC	CC	CC	CC	CC	CC	CC	CC	CC	0.00%	57%	56.70%
	ciw3	CC	CL	CC	CC	CC	CC	CC	CC	CC	CC	CC	CC	CC	CL	CC	CC	CC	CC	5.56%	73%	67.74%
	nga1126	CC	CL	CC	CC	CC	CL	CC	CC	CC	CC	CC	CC	CC	CC	CC	CC	CC	CC	5.56%	60%	54.44%
	nga168	CC	CL	CC	CC	CC	CL	CC	CC	CC	CC	CC	CC	CC	CC	CC	CC	CC	CC	5.56%	63%	57.74%
Chr 3	nga162	CC	CL	CL	CC	CL	CL	CL	CL	CC	CL	CC	CC	CL	CC	CC	CL	CC	CC	25.00%	68%	43.30%
	ciw11	CC	CC	CC	CC	CC	CC	CC	CC	CC	CC	CC	CC	CC	CC	CC	CC	CC	CC	0.00%	58%	58.30%
	ciw4	CC	CC	CC	CC	CC	CC	CC	CC	CC	CC	CC	CC	CC	CC	CC	CC	CC	CC	0.00%	40%	40.00%
	nga6	CC	CC	CC	CC	CC	CC	CC	CC	CC	CC	CC	CC	CC	CC	CC	CC	CC	CC	0.00%	46%	46.70%
Chr 4	ciw5	CC	CL	CC	CC	CL	CC	CL	CC	CL	CL	CC	CC	CL	CC	CC	CL	CL	CC	22.22%	50%	27.78%
	ciw6	CC	CC	CL	CL	CL	CC	CL	CC	CL	CC	CL	CL	CL	CL	CC	CC	CL	CL	30.56%	43%	12.74%
	ciw7	CC	CC	CC	CC	CC	CC	CC	CC	CC	CC	CC	CC	CC	CC	CC	CC	CC	CC	0.00%	38%	38.30%
	nga1107	CC	CL	CC	CC	CC	CL	CC	CL	CC	CC	CC	CC	CC	CC	CC	CC	CC	CC	8.33%	30%	21.67%
Chr 5	CTR1	CC	CC	CC	CC	CC	CC	CC	CC	CC	CC	CC	CC	CC	CC	CC	CC	CC	CC	0.00%	0%	0.00%
	ciw8	CC	CC	CC	CC	CC	CC	CC	CC	CC	CC	CC	CC	CC	CC	CC	CC	CC	CC	0.00%	0%	0.00%
	PHYC	CL	CL	CC	CC	CC	CL	CC	CL	CC	CC	CC	CC	CC	CL	CC	CL	CC	CC	16.67%	60%	43.33%
	ciw9	CL	CL	CL	CC	CL	CL	CL	CL	CL	CC	CL	CL	CL	CC	CL	CC	CC	CC	36.11%	65%	28.89%
	ciw10	CL	CL	CC	CC	CC	CL	CC	CL	CC	CC	CL	CC	CC	CL	CC	CL	CC	CC	19.44%	67%	47.26%

Figure 2-5. Result of BC5 F1 mapping.

30 plants, that were self-pollinated after one backcross of L*er* dme-2 homozygote and Col-*gl* dme-2 heterozygote, were mapped. List of markers is the leftmost column, and the number in rightmost column represents Ler ratio for each marker locus. Red box; locus with L*er* ratio of over 20% in BC5 F1 or 10% higher than average in BC1 F2, orange box; locus with difference between BC1 F2 and BC5 F1 less than 30%, CC; Col/Col, CL; Col/L*er*.

2.3.3. Mutant allele of DNA demethylase family gene can rescue dme-mediated seed abortion partially, and abolish the rescue.

DME, the cytosine demethylase of Arabidopsis, has three homologues, *ROS1*, *DML2* and *DML3*. All these family genes are known to be broadly expressed in the sporophytic tissue. However, the triple mutant *ros1*; *dml2*; *dml3* (hereafter *rdd*, Col background) which shows increased DNA methylation throughout the genome do not display any noticeable developmental phenotypes (Penterman et al. 2007). Whereas dme mutant has a defect during reproductive stage (maternal dme mutant allele causes seeds abort), any overt vegetative phenotypes have not been reported yet. Since there are four family members in Arabidopsis genome and there is a possibility of genetic or functional redundancy among these homologues, a generation of quadruple knock-out mutant is required. *DME*, *ROS1*, *DML2*, and *DML3* are located in different chromosomes, thus, they are not linked (figure 2-3). I crossed *rdd* female plants with *dme-2* homozygous pollen in Col-*gl* background (Figure 2-6). The *dme-2* mutant allele in Col-

gl ecotype has a reduced male transmission ratio; only 10-15 % of the segregation population is *DME*/*dme-2*. If *DME*/*dme-2* is self-pollinated and the rest of 85-90 % are all WT(Schoft et al. 2011). This phenomenon reappeared in *rdd*; *DME*/*dme-2* mutants. No quadruple knock-out mutant was obtained from *rdd*; *DME*/*dme-2* self-pollination.

Figure 2-6.

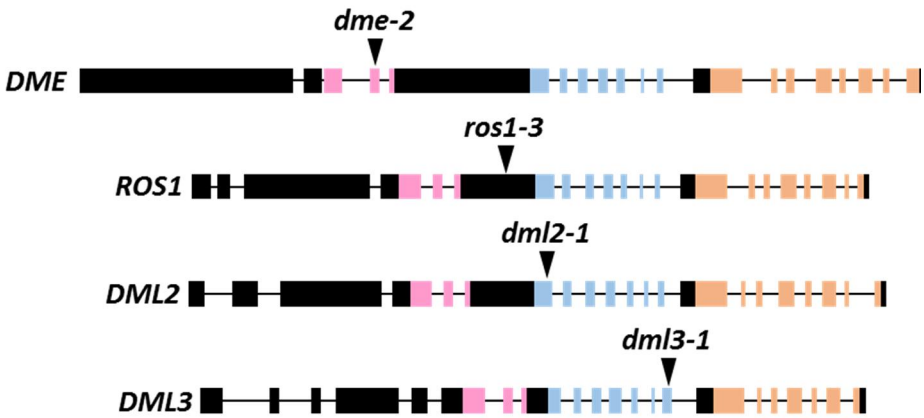

Figure 2-6. Gene diagrams of the DME family members.

Boxed regions are exons, and lines are introns. Blue exons encode the helix–hairpin–helix DNA glycosylase domain, and pink and orange exons encode conserved domains, that are essential for enzyme function(Mok et al. 2010). Black exons encode amino acids not shared between DML proteins. The position of *ros1–3*, *dml2–1*, and *dml3–1* T-DNA insertions is marked by a triangle.

Therefore, I decided to use *dme-2* allele in L*er* background because L*er dme-2* allele shows normal male transmission ratio. Female L*er dme-2* homozygote was crossed with *dme-2* Col-*gl* heterozygous pollen as a control. The male transmission ratio of the *dme-2* allele of this type of cross was still 10 to 15%. But in case of cross between L*er dme-2* homozygous female and *rdd*; *DME*/*dme-2* male in Col-*gl* male, 7 out of 430 individuals were *dme-2* homozygous genotype (L*er*/Col-*gl*). This indicates the male transmission of the *dme-2* allele dropped to 3%. This suggests that *rdd* alleles in male gametes may affect transmission of *dme-2* allele. It is possible that pollen viability or subsequent pollen germination might be defected in quadruple mutant gametes. (Figure 2-7)

Figure 2-7.

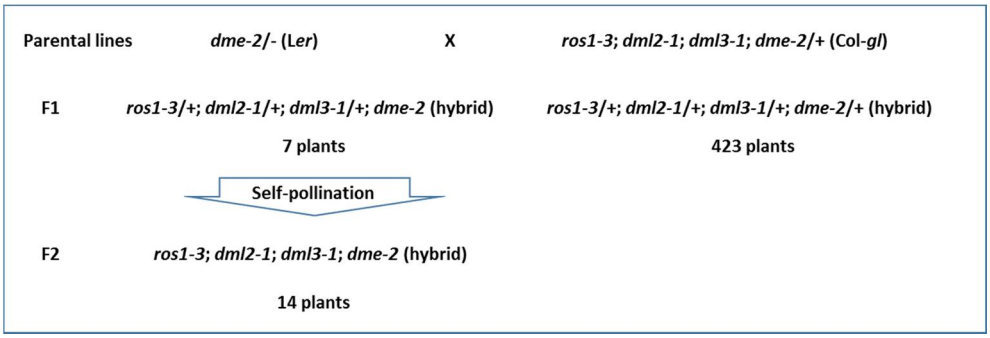

F2 plant #	*dme* (5G04560)	*ros1* (2G36490)	*dml2* (3G10010)	*dml3* (4G34060)
1	ho	he	he	ho
2	ho	wt	wt	he
3	ho	wt	wt	he
4	ho	he	he	ho
5	ho	he	wt	ho
6	ho	wt	he	he
7	ho	ho	he	he
8	ho	he	wt	wt
9	ho	he	he	ho
10	ho	wt	he	ho
11	ho	he	he	wt
12	ho	he	wt	ho
13	ho	he	he	ho
14	ho	he	he	he
Mut/total	28/28	11/28	9/28	17/28

Figure 2-7. Strategy and Progress of quadruple homozygous mutant of DME and DME family genes.

Seven plants with the ros1-3; dml2-1; dml3-1; dme-2/+ genotype of the F1 population did not show abnormal phenotypes in sporophytic tissues except hybrid viability. But only 14 of the seeds of these 7 plants germinated.

From these seven individuals, 14 viable F2 plants were obtained. Theoretically and empirically, the transmission ratio of *ros1-3*, *dml2-1* and *dml3-1* alleles should be all 50%. But the transmission ratio of *ros1-3* and *dml-2* alleles decreased to 39% and 32%, respectively, while *dml3-1* alleles increased to 61% (Figure 2-7). This phenomenon persisted in the next generation produced by F2 with various genotypes (Figure 2-8). Genotype distributions in F3 were also different from empirical results. The expectation was to have 25% of homozygote and 50% of heterozygote segregation for each allele. However, in case of *ros1-3*, only 5% of homozygotes and 26% of heterozygotes were obtained. In case of *dml2-1*, only 1% of homozygous plants and 52% of heterozygous plants were obtained. Interestingly, *dml3-1* showed increased allele transmission; 73% homozygotes and 20% heterozygotes. This infers that the transmission of *ros1-3* and *dml2-1* is reduced when they co-exist with dme mutant allele. Both *ros1-3* and *dml2-1* seem to lower the seed viability of *dme-2*. By contrast, *dml3-1* homozygous state seems to ameliorate the

poor seed viability of *dme-2* mutant. The increased seed viability via *dml3-1* allele was observed even in *dml3-1* heterozygous state. Seed viability of *dme-2* homozygote was 3% (seed abortion ratio 97%), but heterozygous for *dml3-1* and homozygous for *dme-2* allele showed 13% of seed viability (seed abortion ratio 87%). Seed viability of *dme-2 dml3-1* double homozygous mutants was 18% (seed abortion ratio 82%). Since the seed viability of homozygous *dme-2* is basically low, mutation in *ROS1* and *DML2* caused additive effect on *dme-2*-mediated seed abortion. When *ros1-3* or *dml2-1* allele is segregated together with *dme-2*; *dml3-1* double homozygous state showing 82% seed abortion, its seed abortion ratio increased to 91% and 100%, respectively. Furthermore, the seed abortion ratio increased when *ros1-3* and *dml2-1* is homozygous than of heterozygous. This suggests that all these mutant alleles show gametophytic effect on seed viability (Figure 2-10).

Figure 2-8.

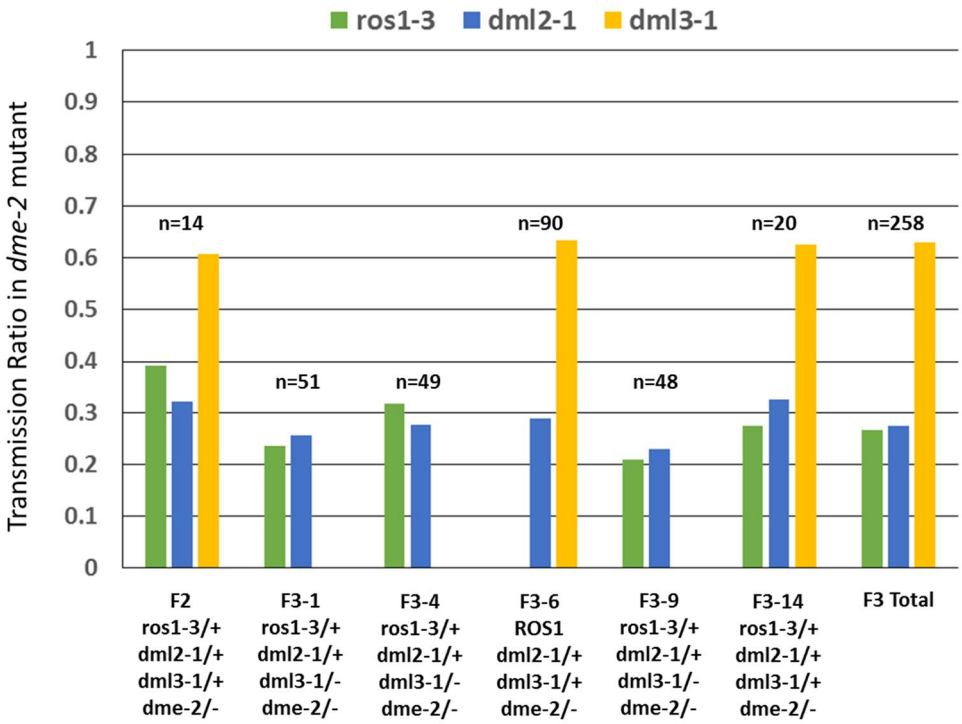

Figure 2-8. Transmission ratio of DME family gene mutant alleles.

In *dme-2*, *ros1-3* and *dml2-1* mutants each allele is transmitted at a reduced level compared to wild type, while transmission of *dml3-1* allele was significantly higher than the predicted 50%. Regardless of genotype or generation, the transmission ratio of each mutant allele was constant.

Figure 2-9.

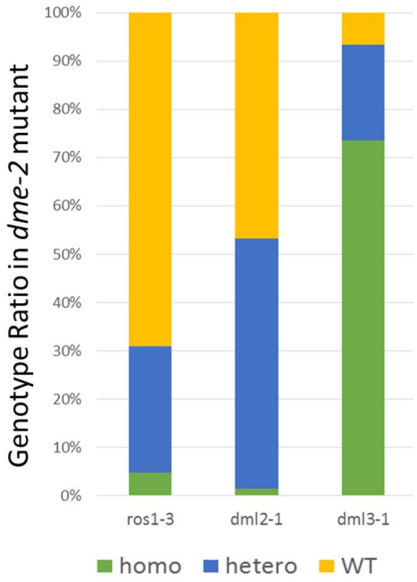

Figure 2-9. Genotype distribution of 258 F3 plants.

ros1-3 has a reduced number of heterozygotes or homozygotes. The heterozygote number of *dml2-1* is normal but few homozygote is obtained, whereas *dml3-1* has a much higher homozygote than expected. Distribution of 3 alleles was also constant regardless of genotype.

Figure 2-10.

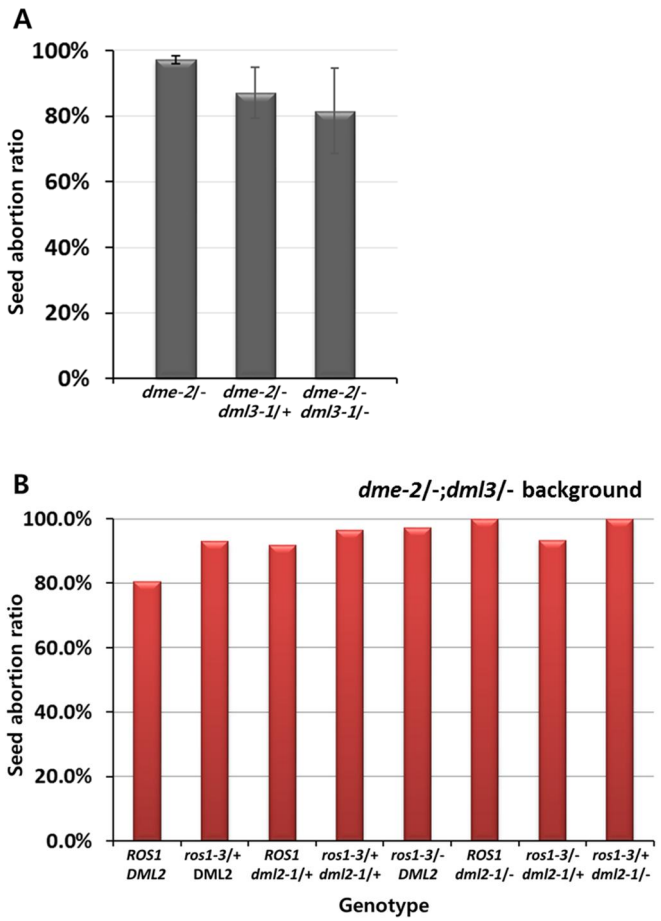

Figure 2-10. *ros1-3*, *dml2-1* and *dml3-1* mutant allele affect seed abortion of *dme-2* homozygote.

(A) dml3-1 mutant alleles can rescue seed abortion of dme-2 mutant, partially. The effect of dml3-1 on seed abortion is dosage-dependent. (*B*) Because seed abortion ratio of dme-2 is up to 97%, effect of ros1-3 or dml2-1 allele on seed abortion is not able to be identified without dme3-1

mutant allele. Therefore, effect of *ros1-3* or *dml2-1* allele was measured in *dme-2*; *dml3-1* double mutant. *ros1-3* and *dml2-1* mutant allele abolish the seed abortion-reducing effects of *dml3-1*. The effect of *ros1-3* and *dml2-1* is synergistic and dosage-dependent.

To investigate the effect of *dml3-1* allele on seed development, I compared seeds of *dme-2* with *dme-2*; *dml3-1* double mutants. I selected 25-30th silique from the inflorescence and observed the embryo inside the seeds to check its developmental stage under a microscope. As a result, *dme-2*; *dml3-1* double mutant seeds were slightly more developed than *dme-2* seeds. Specifically, only 10 % of *dme-2* seeds developed further than inter heart-torpedo, but 42 % of double mutant seeds were in the inter heart-torpedo or beyond that stage (Figure 2-11). This clearly suggests that *dml3-1* mutation increased *dme-2* seed viability.

Only one quadruple homozygote was obtained from more than 400 F3 plants. This particular plant exhibited a bushy phenotype, had more axillary stems and a lot of flowers. But the flowers failed to develop into siliques and no viable seeds were obtained.

Figure 2-11.

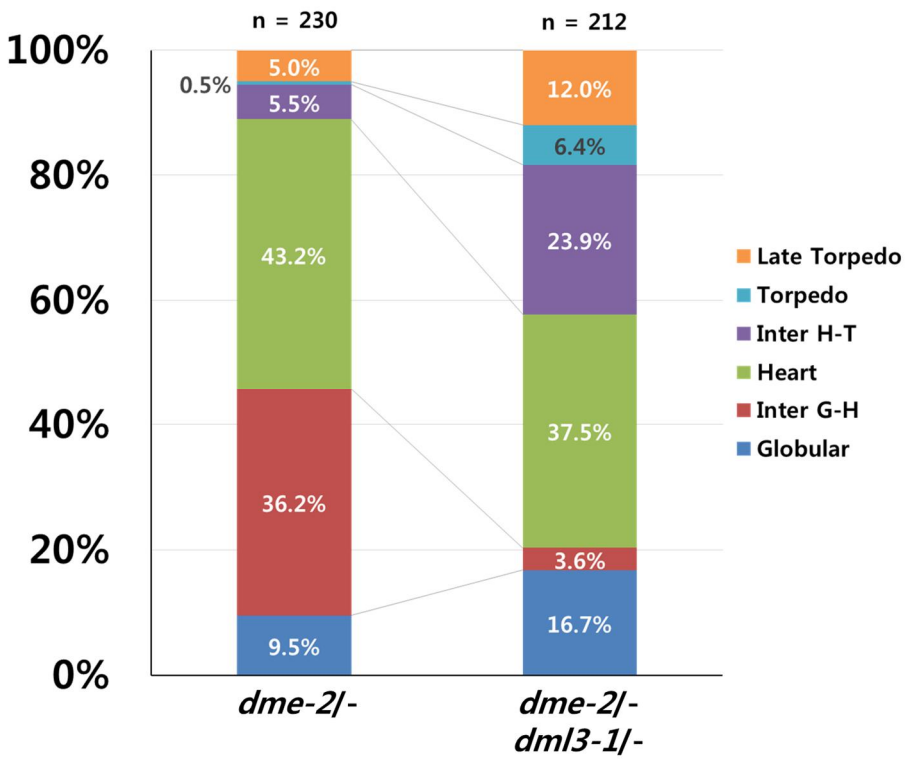

Figure 2-11. Comparison of developmental stage between *dme-2* embryo and *dme-2* & *dml3-1* double mutant embryo.

Comparing the proportion of each stage, *dme-2* mutant embryo usually stops at heart stage and only a small number of seeds proceed further development. On the other hand, *dme-2* & *dml3-1* double mutant seeds in post-heart stage takes a considerable proportion.

Figure 2-12.

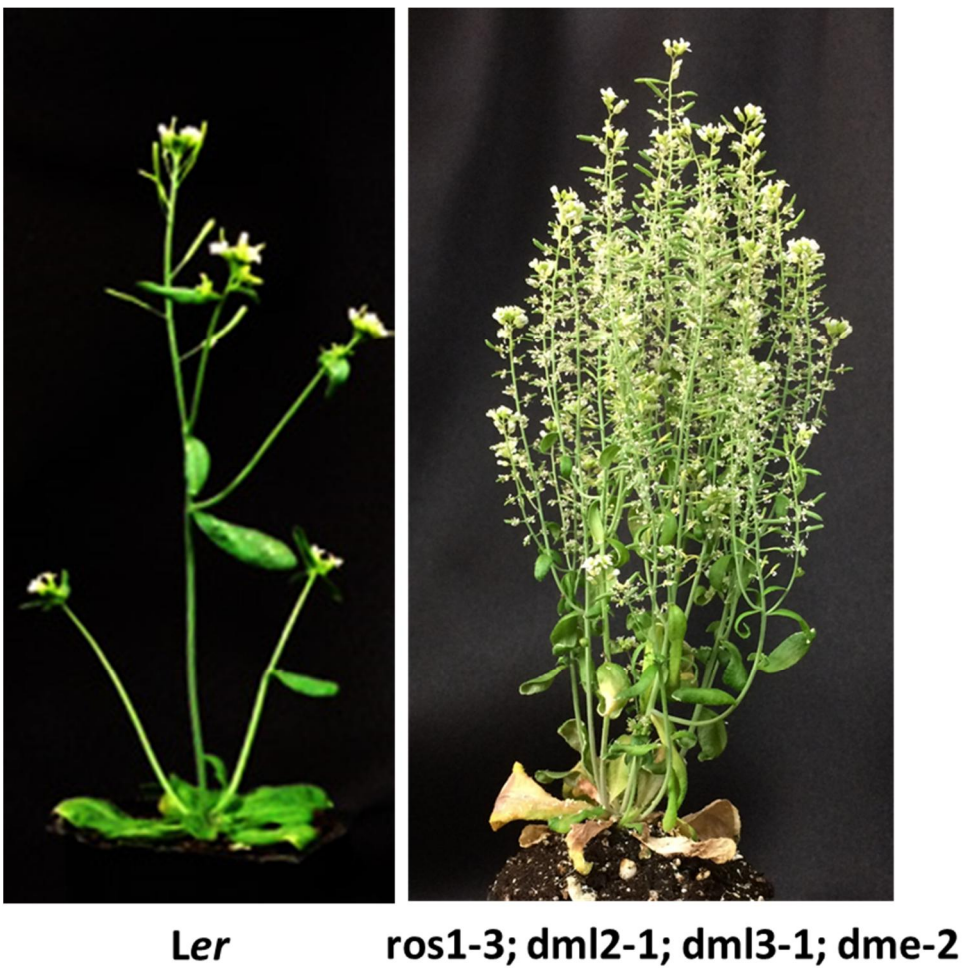

Figure 2-12. One quadruple mutant was obtained.

Of the 400 individuals I identified genotype, there was one quadruple mutant. The quadruple mutants seemed to lost apical dominance. It had many stems and flowers than wild-type. Unfortunately, next generation of the quadruple mutant was not obtained, because it was sterile,

2.3.4. It is altered that interaction of *ros1-3*, *dml2-1* and *dml3-1* in *+46 cDME*; *dme-2* Col background

In order to construct *rdd*; *dme-2* quadruple mutants without ecotype issue, I crossed *rdd dme-2*/+ mutant with Col-gl *dme-2* mutant with *+46 cDME*. The +46cDME transgene is expressed only in the central cell, but not in other sporophytic tissues. Therefore, I can assume that in *dme-2* mutants with *+46 cDME* transgene, the seeds are viable during reproductive stage owing to the active DME transgene. Because this *+46 cDME* transgene is not active during vegetative growth, I can expect the vegetative effect of *dme-2* allele remains, if any. F1 was self-pollinated to produce 411 F2. And the self-fertilized F2 produced 537 F3. All these 411 F2 and 537 F3 plants were genotyped to find quadruple mutant and other transmission effects.

The transmission ratio of *ros1-3* in F2 population was 46%, and *dml2-1* and *dml3-1* were 41% and 59%, respectively. Compared to L*er* / Col-*gl* hybrid, *ros1-3* and *dml2-1* did increase, but *dml3-1* was still near 60%.

The genotype distribution was also different from the hybrid. The heterozygous plant ratio was 52% in *ros1-3* and *dml2-1* which is close to empirical expectations. However homozygous plant ratio was 19% and 15%, respectively, which is higher than hybrid but still lower than 25%. *dml3-1* allele showed 21.5% homozygote and 75% heterozygote ratio, which is obviously different from that of *ros1-3*/+; *dml2-1*/+; *dml3-1*/+ triple heterozygote (Figure 2-9 and 2-13).

Figure 2-13.

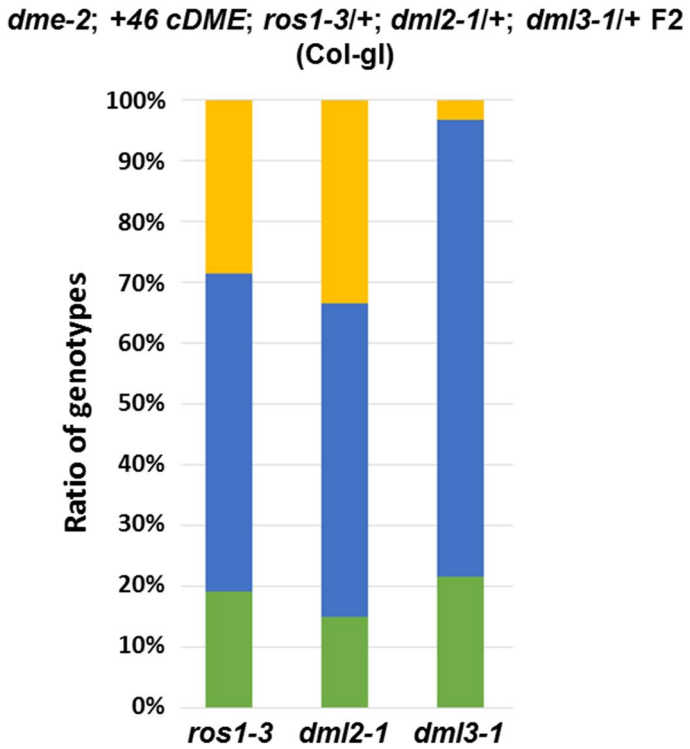

Figure 2-13. Genotype distribution of F2 population

As results of cross for generating L*er*/Col hybrid quadruple mutants, transmission ratio of *dml3-1* mutant allele is higher other two mutant alleles (*ros1-3* and *dml2-1*). However, portion of *dml3-1* homozygote reduced. In contrast homozygote and heterozygote of *ros1-3*, *dml-2* are increased (Still portion of homozygote is lower than 25%).

F3 showed another pattern. The *ros1-3* transmission ratio increased from 46% (F2) to 58% (F3). And the *dml2-1* transmission increased slightly from 41% to 46%. The *dml2-1* allele transmission, which was 59% in F2 decreased in 48%. Since the genotypes of F2 are diverse, F3 data of identical mutants were gathered to analyze the overall allele transmission ratio to determine any genetic correlation between mutant alleles.

Within the *+46 cDME*; *dme-2* background, *ros1-3* transmission ratio was 24% by homozygous *dml3-1* but 60% by homozygous *dml2-1*. The *dml2-1* allele showed 41% transmission with the *ros1-3* homozygote but 50% with *dml2-1* homozygote. And *dml3-1* allele was delivered in 54% of *ros1-3* homozygote and 35% in *dml2-1* homozygote.

In summary, the transmission ratio between any two genes was not complementary. And each *ros1-3*, *dml2-1* and *dml3-1* alleles seem to form a cyclic relationship. (Figure 2-14) This phenomenon might be a part of the reason why no single quadruple mutant was obtained from 900 F2 and F3 plants. Rarely, Some of the F2 individuals displayed late flowering

phenotype.

Figure 2-14.

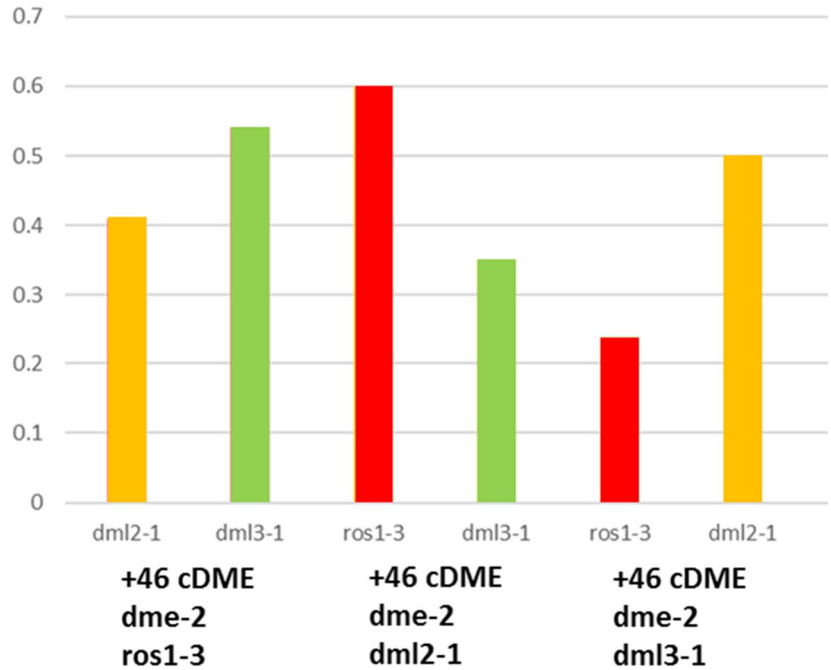

Figure 2-14. Transmission ratio of DNA demethylase mutant allele altered by its genotype.

Unlike the experiment for generating L*er*/Col hybrid quadruple mutants, *ros1-3* and *dml2-1* alleles could be transmitted over 50% in some genotypes. And the transmission ratio of *dml3-1* allele was decreased by 35% in *+46 cDME*; *dme-2*; *ros1-3* background.

Furthermore, these plants showed other phenotypes such as early primary shoot termination, short silique and a defect in pollen dehiscence. Five out of these six plants were *+46 cDME*; *dme-2*; *ros1-3* homozygote. As these plant exhibits late flowering phenotype (Figure 2-15), *FWA* expression levels were examined with RNA extracted from rosette leaves. *FWA* expression was proportional only to the degree of late flowering phenotype (Figure 2-16). Offspring of the plants, show late flowering phenotype, were obtained hardly because of a defect in pollen dehiscence. And no plant, that was obtained from late flowering plants, showed abnormal phenotypes. On the other hand, some offspring of plants with normal flowering phenotype did show late flowering.

Figure 2-15.

Figure 2-15. A little number of plants in F2 and F3 show late flowering. Six out of 400 plants show late flowering. Also, these plants show early termination of primary shoot apical meristem, defect of pollen release and short siliques in common. But their progenies lose the phenotypes. On the other hand, other plants, that is offspring of plants without any phenotype, gain the phenotype mentioned above.

Figure 2-16.

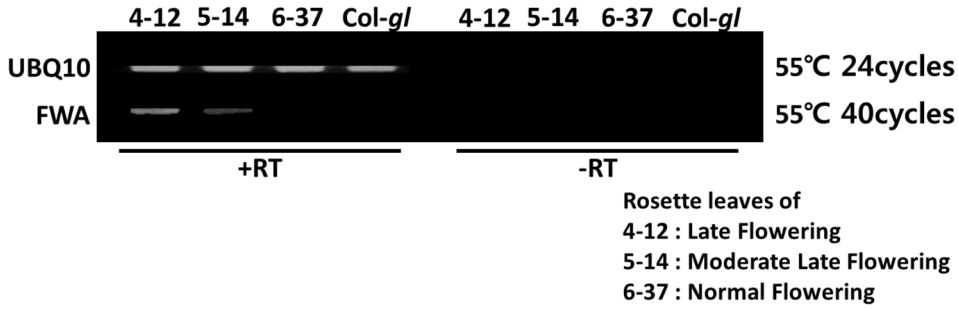

Figure 2-16. Expression of *FWA* gene.

The expression of the FWA gene is consistent with the late flowering phenotype**.**

2.4 Discussion

In this study, I have presented genetic data derived from mutant crosses of the DNA demethylase homologues. Several studies have reported that DNA methylation pattern disappears genome-wide when the function of *MET1* is lost (Zhang and Jacobsen 2006; Cokus et al. 2008). *MET1* methyl transferase is known to be involved in maintaining CG methylation. Gene expression profiles and various phenotypes resulted from the dramatic CG methylation change due to the lack of met1 mutation have long been discovered (Zilberman and Henikoff 2007). By contrast, combinational mutant analyses of *DME*, *ROS1*, *DML2*, and *DML3*, which act as counter-part of *MET1*, have not been extensively studied yet.

I believe that the genetic data derived from this study, has provided an insight into the relationship and the function of DNA demethylases.

I have shown that the increased seed viability of the L*er dme-2* which has been in homozygous state over generations came back to the original high abortion phenotype by crossing it with the dme heterozygote. The high lethality during seed development process acts as a strong selection bias, suggesting that the promoted genetic or epigenetic change in the population is reduced by crosses between individuals that were not under bias. It is plausible to think that the epigenetic change has occurred in *dme* mutants and perhaps it might be accumulated over the generations. If this is a genetic change, the phenotypic changes should be maintained to the same levels during crosses or over the generations. The fascinating fact is that two generations were needed to revert this epigenetic change. In the F1 obtained through the cross between homozygous *dme-1* (higher seed viability) and *dme-2* heterozygote, either dme-1 heterozygote or *dme-1*/*dme-2* hybrid homozygote had still higher numbers of viable seeds than reported. In the F2 generation on the other hand, now showed high seed abortion as they were originally found. The reason why *dme* mutant takes

2 generations to recover their phenotype or epigenetic status is difficult to explain clearly. But it seems hard for accumulated epigenetic status is changed by mixing with other genome in a short time. Furthermore, the plant getting original phenotype is still dme-1/dme-2 hybrid mutant. And in plants, patterns of DNA methylation are stably maintained through sexual reproduction (Cubas et al. 1999) (Saze, Mittelsten Scheid, and Paszkowski 2003) (Manning et al. 2006) (Paszkowski and Grossniklaus 2011).

I could find a preference in the genome inheritance of the dme-2 mutant in viable seeds, during the cross between L*er dme-2* homozygote and Col-*gl dme-2* heterozygote. In both mappings of BC1 F2 and BC5 F1, there were regions showing highly L*er*-originated genome content than others. One was the marker nga162 of the chromosome 3 upper arm and the other was located in the lower arm of the chromosome 5. The lower arm of chromosome 5 contains *MET1*, the counterpart of the DME. However, it was reported that transcription level of *MET1* is not correlated

with DNA methylation on its promoter (Ashapkin, Kutueva, and Vanyushin 2011). Considering the lethality of the dme mutant, this asymmetric genome inheritance may be due to the reproduction process. As a backcross had been successive, since BC3, the asymmetric transmission might be caused by the female gamete. But it is not certain whether it is a gametophytic effect or a sporophytic effect in the seed developmental process. It is obviously not due to the male transmission defect of the Col-*gl* dme mutant. The chromosome 2 region, which has shown higher L*er* content in BC1 F2 but lowered in BC5, was the site of *ERECTA* gene. The reason for the high L*er* ratio in the vicinity of *ERECTA* of BC1 mapping seems to be due to the difference in silique structure by ecotype and the low dme mutant male transmission in Col-*gl* background. Comparing the seed abortion pattern of BC1 F2 with the overall appearance of the plants, 88% of L*er*-type plants showed seed abortion, while 95% of the Col-*gl* type plants had seed abortion. While the backcrosses were progressed without selfing since BC3, the chromosome

2 imbalance seemed to disappear as the L*er*-appearance bias vanished. Other regions that still had more than 20% of L*er*-content in BC5 was ciw12, nga111 of the chromosome 1 and ciw5, ciw6 located in chromosome 4. These regions were not predominant in any ecotype in BC1 F2, but half or more of the female gametes delivered to BC5 had L*er* genomes. As a result, the reason why multiple L*er*-high regions exist up to BC5 is thought to be due to the multiple loci from L*er* affecting the viability of dme seeds.

The seed abortion of the Col-*gl* / L*er* hybrid background dme mutant was reduced by the *dml3* mutation and increased again by *ros1-3* or *dml2-1*.

The decrease in seed abortion by the *dml3-1* and the increase by the *ros1-3* and *dml2-1* were all observed in heterozygous and increased in homozygous.

This may be considered to be a gametophytic effect or dosage dependent.

I have shown that some of the *+46 cDME*; *dme-2*; *ros1-3* mutants

with late-flowering phenotype had a correlation with the *FWA* gene expression.

However, unlike the previously reported *fwa* epi-allele, the phenotype was not maintained in the next generation (Kakutani 1997).

The *fwa* epi-allele produced by the *ddm1* or *met1-1* mutations are stable and transmissible (Kakutani 1997) (Soppe et al. 2000). The difference between the *fwa* epi mutant and the late flowering *+46 cDME*; *dme-2*; *ros1-3* mutant is that they show early termination of the primary shoot apical meristem, overgrowth of the secondary branch and the short silique due to the pollen release defect.

All six individuals with late flowering showed the same phenotype, leaving very few seeds, but all phenotypes disappeared in the next generation.

The reason for the disappearance of the phenotype may be because of the instability of the acquired epigenetic trait. But there is also a possibility that the seed viability was lowered by other factors so that it could not be

delivered.

Early termination of the primary shoot apical meristem and overgrowth of the secondary branch was identified in the subunits of the Elongator complex in Arabidopsis, *elo1*, *elo2*, *elo3* and their target *shy2* mutant. *SHY2* which is a transcription factor involved in the auxin response, may be related to the auxin signal (Nelissen et al. 2010).

III. References

Ariel, F. D., P. A. Manavella, C. A. Dezar, and R. L. Chan. 2007. 'The true story of the HD-Zip family', *Trends Plant Sci*, 12: 419-26.

Ashapkin, VV, LI Kutueva, and BF %J Russian journal of genetics Vanyushin. 2011. 'Is the cytosine DNA methyltransferase gene MET1 regulated by DNA methylation in Arabidopsis thaliana plants?', 47: 279-88.

Berger, N., B. Dubreucq, F. Roudier, C. Dubos, and L. Lepiniec. 2011. 'Transcriptional regulation of Arabidopsis LEAFY COTYLEDON2 involves RLE, a cis-element that regulates trimethylation of histone H3 at lysine-27', *Plant Cell*, 23: 4065-78.

Boavida, L. C., F. Borges, J. D. Becker, and J. A. Feijo. 2011. 'Whole genome analysis of gene expression reveals coordinated activation of signaling and metabolic pathways during pollen-pistil interactions in Arabidopsis', *Plant Physiol*, 155: 2066-80.

Borges, F., G. Gomes, R. Gardner, N. Moreno, S. McCormick, J. A. Feijo, and J. D. Becker. 2008. 'Comparative transcriptomics of Arabidopsis sperm cells', *Plant Physiol*, 148: 1168-81.

Chan, R. L., G. M. Gago, C. M. Palena, and D. H. Gonzalez. 1998. 'Homeoboxes in plant development', *Biochim Biophys Acta*, 1442: 1-19.

Charite, J., W. de Graaff, D. Consten, M. J. Reijnen, J. Korving, and J. Deschamps. 1998. 'Transducing positional information to the Hox genes: critical interaction of cdx gene products with position-sensitive regulatory elements', *Development*, 125: 4349-58.

Choi, Y., M. Gehring, L. Johnson, M. Hannon, J. J. Harada, R. B. Goldberg, S. E. Jacobsen, and R. L. Fischer. 2002a. 'DEMETER, a DNA glycosylase domain protein, is required for endosperm gene imprinting and seed viability in Arabidopsis', *Cell*, 110: 33-42.

Cokus, S. J., S. Feng, X. Zhang, Z. Chen, B. Merriman, C. D. Haudenschild, S. Pradhan, S. F. Nelson, M. Pellegrini, and S. E. Jacobsen. 2008. 'Shotgun bisulphite sequencing of the Arabidopsis genome reveals DNA methylation patterning', *Nature*, 452: 215-9.

Crooks, G. E., G. Hon, J. M. Chandonia, and S. E. Brenner. 2004. 'WebLogo: a

sequence logo generator', *Genome Res*, 14: 1188-90.

Cubas, A., J. C. Herrero, E. Morales, A. Carreno, B. Dominguez-Gil, A. Cirujeda, M. Praga, T. Ortuno, E. Hernandez, M. Delgado, A. Andres, and J. M. Morales. 1999. 'The early impact of mycophenolate mofetil in combination with steroids and cyclosporine Neoral after renal transplantation: a six-month analysis', *Transplant Proc*, 31: 2265-6.

Drews, G. N., and A. M. Koltunow. 2011. 'The female gametophyte', *Arabidopsis Book*, 9: e0155.

Gehring, M., J. H. Huh, T. F. Hsieh, J. Penterman, Y. Choi, J. J. Harada, R. B. Goldberg, and R. L. Fischer. 2006. 'DEMETER DNA glycosylase establishes MEDEA polycomb gene self-imprinting by allele-specific demethylation', *Cell*, 124: 495-506.

Gehring, M., V. Missirian, and S. Henikoff. 2011. 'Genomic analysis of parent-of-origin allelic expression in Arabidopsis thaliana seeds', *PLoS One*, 6: e23687.

Gong, Z., T. Morales-Ruiz, R.R. Ariza, T. Roldan-Arjona, L. David, and J.-J. Zhu. 2002. 'ROS1, a Repressor of Transcriptional Gene Silencing in Arabidopsis, Encodes a DNA Glycosylase/Lyase', *Cell*, 111: 803-14.

Grossniklaus, U., J. P. Vielle-Calzada, M. A. Hoeppner, and W. B. Gagliano. 1998. 'Maternal control of embryogenesis by MEDEA, a polycomb group gene in Arabidopsis', *Science*, 280: 446-50.

He, X. J., T. Chen, and J. K. Zhu. 2011. 'Regulation and function of DNA methylation in plants and animals', *Cell Res*, 21: 442-65.

Hehenberger, E., D. Kradolfer, and C. Kohler. 2012. 'Endosperm cellularization defines an important developmental transition for embryo development', *Development*, 139: 2031-9.

Hilderson, D., A. S. Saidi, K. Van Deyk, A. Verstappen, A. H. Kovacs, S. M. Fernandes, M. M. Canobbio, D. Fleck, A. Meadows, R. Linstead, and P. Moons. 2009. 'Attitude toward and current practice of transfer and transition of adolescents with congenital heart disease in the United States of America and Europe', *Pediatr Cardiol*, 30: 786-93.

Hsieh, T. F., C. A. Ibarra, P. Silva, A. Zemach, L. Eshed-Williams, R. L. Fischer, and D. Zilberman. 2009. 'Genome-wide demethylation of Arabidopsis

endosperm', *Science*, 324: 1451-4.

Hsieh, T. F., J. Shin, R. Uzawa, P. Silva, S. Cohen, M. J. Bauer, M. Hashimoto, R. C. Kirkbride, J. J. Harada, D. Zilberman, and R. L. Fischer. 2011. 'Regulation of imprinted gene expression in Arabidopsis endosperm', *Proc Natl Acad Sci U S A*, 108: 1755-62.

Ibarra, C. A., X. Feng, V. K. Schoft, T. F. Hsieh, R. Uzawa, J. A. Rodrigues, A. Zemach, N. Chumak, A. Machlicova, T. Nishimura, D. Rojas, R. L. Fischer, H. Tamaru, and D. Zilberman. 2012. 'Active DNA demethylation in plant companion cells reinforces transposon methylation in gametes', *Science*, 337: 1360-4.

Jeddeloh, J. A., T. L. Stokes, and E. J. Richards. 1999. 'Maintenance of genomic methylation requires a SWI2/SNF2-like protein', *Nat Genet*, 22: 94-7.

Kakutani, T. 1997. 'Genetic characterization of late-flowering traits induced by DNA hypomethylation mutation in Arabidopsis thaliana', *Plant J*, 12: 1447-51.

Kim, M., H. Ohr, J. W. Lee, Y. Hyun, R. L. Fischer, and Y. Choi. 2008. 'Temporal and Spatial Downregulation of Arabidopsis MET1 Activity Results in Global DNA Hypomethylation and Developmental Defects', *Molecules and Cells*, 26: 611-15.

Kohler, C., L. Hennig, R. Bouveret, J. Gheyselinck, U. Grossniklaus, and W. Gruissem. 2003. 'Arabidopsis MSI1 is a component of the MEA/FIE Polycomb group complex and required for seed development', *Embo J*, 22: 4804-14.

Kooiker, M., C. A. Airoldi, A. Losa, P. S. Manzotti, L. Finzi, M. M. Kater, and L. Colombo. 2005. 'BASIC PENTACYSTEINE1, a GA binding protein that induces conformational changes in the regulatory region of the homeotic Arabidopsis gene SEEDSTICK', *Plant Cell*, 17: 722-9.

Law, J. A., and S. E. Jacobsen. 2010. 'Establishing, maintaining and modifying DNA methylation patterns in plants and animals', *Nat Rev Genet*, 11: 204-20.

Luo, M., P. Bilodeau, E. S. Dennis, W. J. Peacock, and A. Chaudhury. 2000. 'Expression and parent-of-origin effects for FIS2, MEA, and FIE in the endosperm and embryo of developing Arabidopsis seeds', *Proc Natl*

Acad Sci U S A, 97: 10637-42.

Manning, K., M. Tor, M. Poole, Y. Hong, A. J. Thompson, G. J. King, J. J. Giovannoni, and G. B. Seymour. 2006. 'A naturally occurring epigenetic mutation in a gene encoding an SBP-box transcription factor inhibits tomato fruit ripening', *Nat Genet*, 38: 948-52.

Martínez, Germán, Kaushik Panda, Claudia Köhler, and R. Keith Slotkin. 2016. 'Silencing in sperm cells is directed by RNA movement from the surrounding nurse cell', *Nature Plants*: 16030.

Matzke, M. A., and R. A. Mosher. 2014. 'RNA-directed DNA methylation: an epigenetic pathway of increasing complexity', *Nat Rev Genet*, 15: 394-408.

Merkley, M. A., E. Hildebrandt, R. H. Podolsky, H. Arnouk, D. G. Ferris, W. S. Dynan, and H. Stoppler. 2009. 'Large-scale analysis of protein expression changes in human keratinocytes immortalized by human papilloma virus type 16 E6 and E7 oncogenes', *Proteome Sci*, 7: 29.

Mok, Y. G., R. Uzawa, J. Lee, G. M. Weiner, B. F. Eichman, R. L. Fischer, and J. H. Huh. 2010. 'Domain structure of the DEMETER 5-methylcytosine DNA glycosylase', *Proc Natl Acad Sci U S A*, 107: 19225-30.

Monfared, M. M., M. K. Simon, R. J. Meister, I. Roig-Villanova, M. Kooiker, L. Colombo, J. C. Fletcher, and C. S. Gasser. 2011. 'Overlapping and antagonistic activities of BASIC PENTACYSTEINE genes affect a range of developmental processes in Arabidopsis', *Plant J*, 66: 1020-31.

Morales-Ruiz, T., A.P. Ortega-Galisteo, M.I. Ponferrada-Marin, R.R. Martinez-Macias, R. R. Ariza, and T. Roldan-Arjona. 2006. 'DEMETER and REPRESSOR OF SILENCING1 encode 5-methylcytosine DNA glycosylases', *Proc Natl Acad Sci U S A*, 103: 6853-58.

Nelissen, Hilde, Steven De Groeve, Delphine Fleury, Pia Neyt, Leonardo Bruno, Maria Beatrice Bitonti, Filip Vandenbussche, Dominique Van Der Straeten, Takahiro Yamaguchi, and Hirokazu %J Proceedings of the National Academy of Sciences Tsukaya. 2010. 'Plant Elongator regulates auxin-related genes during RNA polymerase Ⅱ transcription elongation', 107: 1678-83.

Niki, S., K. Haruyama, S. Kokuno, T. Itoi, T. Mizoue, K. Takei, Y. Mizumura, J.

Sanada, Y. Mizuguchi, S. Ogihara, K. Takeda, K. Onoda, K. Miwa, Y. Shinohara, Y. Magami, T. Horibe, H. Kakutani, T. Niido, T. Seki, T. Hisa, and T. Saitou. 1997. '[A case of hepatocellular carcinoma associated with autoimmune hepatitis and increased scintigraphy of liver accumulation]', *Nihon Shokakibyo Gakkai Zasshi*, 94: 220-4.

O'Malley, R. C., S. S. Huang, L. Song, M. G. Lewsey, A. Bartlett, J. R. Nery, M. Galli, A. Gallavotti, and J. R. Ecker. 2016. 'Cistrome and Epicistrome Features Shape the Regulatory DNA Landscape', *Cell*, 165: 1280-92.

Ortega-Galisteo, A.P., T. Morales-Ruiz, R.R. Ariza, and T. Roldan-Arjona. 2008. 'Arabidopsis DEMETER-LIKE proteins DML2 and DML3 are required for appropriate distribution of DNA methylation marks', *Plant Mol Biol*, DOI 10.1007/s11103-008-9346-0.

Palena, C. M., D. H. Gonzalez, and R. L. Chan. 1999. 'A monomer-dimer equilibrium modulates the interaction of the sunflower homeodomain leucine-zipper protein Hahb-4 with DNA', *Biochem J*, 341 (Pt 1): 81-7.

Palena, C. M., A. E. Tron, C. W. Bertoncini, D. H. Gonzalez, and R. L. Chan. 2001. 'Positively charged residues at the N-terminal arm of the homeodomain are required for efficient DNA binding by homeodomain-leucine zipper proteins', *J Mol Biol*, 308: 39-47.

Park, J. S., J. M. Frost, K. Park, H. Ohr, G. T. Park, S. Kim, H. Eom, I. Lee, J. S. Brooks, R. L. Fischer, and Y. Choi. 2017. 'Control of DEMETER DNA demethylase gene transcription in male and female gamete companion cells in Arabidopsis thaliana', *Proc Natl Acad Sci U S A*, 114: 2078-83.

Paszkowski, J., and U. Grossniklaus. 2011. 'Selected aspects of transgenerational epigenetic inheritance and resetting in plants', *Curr Opin Plant Biol*, 14: 195-203.

Penterman, J., D. Zilberman, J. H. Huh, T. Ballinger, S. Henikoff, and R. L. Fischer. 2007. 'DNA demethylation in the Arabidopsis genome', *Proc Natl Acad Sci U S A*, 104: 6752-7.

Pikaard, C. S., J. R. Haag, O. M. Pontes, T. Blevins, and R. Cocklin. 2012. 'A transcription fork model for Pol IV and Pol V-dependent RNA-directed DNA methylation', *Cold Spring Harb Symp Quant Biol*, 77: 205-12.

Portereiko, M. F., A. Lloyd, J. G. Steffen, J. A. Punwani, D. Otsuga, and G. N. Drews. 2006. 'AGL80 is required for central cell and endosperm development in Arabidopsis', *Plant Cell*, 18: 1862-72.

Qin, Y., A. R. Leydon, A. Manziello, R. Pandey, D. Mount, S. Denic, B. Vasic, M. A. Johnson, and R. Palanivelu. 2009. 'Penetration of the stigma and style elicits a novel transcriptome in pollen tubes, pointing to genes critical for growth in a pistil', *PLoS Genet*, 5: e1000621.

Rud, B., J. Hilden, L. Hyldstrup, and A. Hrobjartsson. 2009. 'The Osteoporosis Self-Assessment Tool versus alternative tests for selecting postmenopausal women for bone mineral density assessment: a comparative systematic review of accuracy', *Osteoporos Int*, 20: 599-607.

Sauermann, U., C. Stahl-Hennig, N. Stolte, T. Muhl, M. Krawczak, M. Spring, D. Fuchs, F. J. Kaup, G. Hunsmann, and S. Sopper. 2000. 'Homozygosity for a conserved Mhc class Ⅱ DQ-DRB haplotype is associated with rapid disease progression in simian immunodeficiency virus-infected macaques: results from a prospective study', *J Infect Dis*, 182: 716-24.

Saze, H., O. Mittelsten Scheid, and J. Paszkowski. 2003. 'Maintenance of CpG methylation is essential for epigenetic inheritance during plant gametogenesis', *Nat Genet*, 34: 65-9.

Schneider, T. D., and R. M. Stephens. 1990. 'Sequence logos: a new way to display consensus sequences', *Nucleic Acids Res*, 18: 6097-100.

Schoft, V. K., N. Chumak, Y. Choi, M. Hannon, M. Garcia-Aguilar, A. Machlicova, L. Slusarz, M. Mosiolek, J. S. Park, G. T. Park, R. L. Fischer, and H. Tamaru. 2011. 'Function of the DEMETER DNA glycosylase in the Arabidopsis thaliana male gametophyte', *Proc Natl Acad Sci U S A*, 108: 8042-7.

Sessa, G., G. Morelli, and I. Ruberti. 1993. 'The Athb-1 and -2 HD-Zip domains homodimerize forming complexes of different DNA binding specificities', *Embo J*, 12: 3507-17.

Simonini, S., I. Roig-Villanova, V. Gregis, B. Colombo, L. Colombo, and M. M. Kater. 2012. 'Basic pentacysteine proteins mediate MADS domain complex binding to the DNA for tissue-specific expression of target

genes in Arabidopsis', *Plant Cell*, 24: 4163-72.

Slotkin, R. K., M. Vaughn, F. Borges, M. Tanurdzic, J. D. Becker, J. A. Feijo, and R. A. Martienssen. 2009. 'Epigenetic reprogramming and small RNA silencing of transposable elements in pollen', *Cell*, 136: 461-72.

Soppe, W. J., S. E. Jacobsen, C. Alonso-Blanco, J. P. Jackson, T. Kakutani, M. Koornneef, and A. J. Peeters. 2000. 'The late flowering phenotype of fwa mutants is caused by gain-of-function epigenetic alleles of a homeodomain gene', *Mol Cell*, 6: 791-802.

Sticker, D., M. Rothbauer, S. Lechner, M. T. Hehenberger, and P. Ertl. 2015. 'Multi-layered, membrane-integrated microfluidics based on replica molding of a thiol-ene epoxy thermoset for organ-on-a-chip applications', *Lab Chip*, 15: 4542-54.

Wong, E., B. C. Carleton, D. F. Wright, M. A. Smith, L. Verbeek, C. A. Hildebrand, P. Stannard, R. Vaillancourt, P. Elliot-Miller, C. J. Ross, and M. R. Hayden. 2009. 'Genotypic Approaches to Therapy in Children (GATC): using information technology to improve drug safety', *Stud Health Technol Inform*, 143: 209-14.

Woo, H. R., T. A. Dittmer, and E. J. Richards. 2008. 'Three SRA-domain methylcytosine-binding proteins cooperate to maintain global CpG methylation and epigenetic silencing in Arabidopsis', *PLoS Genet*, 4: e1000156.

Wuest, S. E., K. Vijverberg, A. Schmidt, M. Weiss, J. Gheyselinck, M. Lohr, F. Wellmer, J. Rahnenfuhrer, C. von Mering, and U. Grossniklaus. 2010. 'Arabidopsis female gametophyte gene expression map reveals similarities between plant and animal gametes', *Curr Biol*, 20: 506-12.

Xiao, W. Y., M. Gehring, Y. Choi, L. Margossian, H. Pu, J. J. Harada, R. B. Goldberg, R. I. Pennell, and R. L. Fischer. 2003. 'Imprinting of the MEA polycomb gene is controlled by antagonism between MET1 methyltransferase and DME glycosylase', *Developmental Cell*, 5: 891-901.

Xu, L. L., B. G. Stackhouse, K. Florence, W. Zhang, N. Shanmugam, I. A. Sesterhenn, Z. Zou, V. Srikantan, M. Augustus, V. Roschke, K. Carter, D. G. McLeod, J. W. Moul, D. Soppett, and S. Srivastava. 2000. 'PSGR, a

novel prostate-specific gene with homology to a G protein-coupled receptor, is overexpressed in prostate cancer', *Cancer Res*, 60: 6568-72.

Zhang, H., and J. K. Zhu. 2011. 'RNA-directed DNA methylation', *Curr Opin Plant Biol*, 14: 142-7.

Zhang, X., and S. E. Jacobsen. 2006. 'Genetic analyses of DNA methyltransferases in Arabidopsis thaliana', *Cold Spring Harb Symp Quant Biol*, 71: 439-47.

Zhu, J. K. 2009. 'Active DNA demethylation mediated by DNA glycosylases', *Annu Rev Genet*, 43: 143-66.

Zhu, J., A. Kapoor, V. V. Sridhar, F. Agius, and J. K. Zhu. 2007. 'The DNA glycosylase/lyase ROS1 functions in pruning DNA methylation patterns in Arabidopsis', *Curr Biol*, 17: 54-9.

Zilberman, D., and S. Henikoff. 2007. 'Genome-wide analysis of DNA methylation patterns', *Development*, 134: 3959-65.

IV. Abstract in Korean

국문초록

DEMETER (DME) DNA glycosylase는 base-excision repair pathway를 통해 DNA demethylation을 개시하고 애기장대에서의 생식에 필수적이다. DME-매개 DNA demethylation은 짧고 AT-rich하며 nucleosome이 적은 euchromatic TE 목표로 하며, 인접한 유전자의 발현에 영향을 미치고 배유유전자의 각인을 유도한다. 암배우체에서 *DME* 발현과 그에 따른 게놈 전체 DNA demethylation은 난자의 동반 세포인 중심 세포에 국한된다. 이 연구에서 나는 수배우체의 DME 발현은 정자의 동반 세포인 vegetative cell에 제한되며 발현하는 시기도 정밀하게 제한됨을 밝혔다. 리포터 유전자를 사용하여 DME의 전사 조절 요소를 찾았고, DME 유전자의 조절 인자가 암수배우체의 동반 세포에서의 발현을 제어하는 것을 보였다. 이 조절 인자를 가진 프로모터에 의한 DME의 발현은 dme-2 돌연변이의 종자유산표현형을 극복하고 DME와 관련된 DNA methylation을 회복하기에 충분하다. 이 최소 프로모터에서 나는 DME의 발현에 필요한 enhancer 서열을 발견하고, 공개된 데이터베이스를 통해 이 모티프에 결합할 수 있는 후보 단백질들의 목록을 제시한다. 또한 yeast 2 hybrid 실험을 통해 프로모터의 전사

조절 인자에 BPC와 HD-ZIP 전사 인자가 결합함을 보였다. 이 연구결과는 DNA demethylation이 어떻게 조절되어 유전자각인을 유도하고 유해한 요소인 TE을 효과적으로 제한하는지를 알려준다.

돌연변이 부위와 그 에코 타입에 따라 *dme* 돌연변이 체에는 몇 가지 차이점이 있다. 차이점을 확인하기 위해, 다른 에코 타입을 가진 돌연변이체를 교배 시켰다. 교배의 결과, 나는 종자 유산표현형을 극복하는 데 도움이 될 것으로 보이는 게놈 영역을 발견했다. 애기장대에는 DME의 homologue가 3 개의 존재한다. *REPRESSOR OF SILENCING1* (*ROS1*), *DEMETER-LIKE* (*DML*) 2 놔 3이 그것이다. DNA demethylation이 식물 생애주기에 미치는 영향과 demethylase 사이의 상호 작용을 알기 위해, DNA demethylase들의 돌연변이 체의 교배를 사용했고 그를 통해 DNA homologue 사이의 상호 작용의 증거를 발견하였다.

주요어: DNA demethylase, 배우체 동반세포, 단일세포 특이적인 유전자 발현, 에피유전학, enhancers, 전사 조절 인자,

학 번: 2008-20356